Lithos 198–199 (2014) 184–201

Contents lists available at ScienceDirect

Lithos

journal homepage: www.elsevier.com/locate/lithos

The role of subduction channel mélanges and convergent subduction systems in the petrogenesis of post-collisional K-rich mafic magmatism in NW Tibet

Zhengfu Guo [a,*], Marjorie Wilson [b], Lihong Zhang [a], Maoliang Zhang [a], Zhihui Cheng [a], Jiaqi Liu [a]

[a] Key Laboratory of Cenozoic Geology and Environment, Institute of Geology and Geophysics, Chinese Academy of Sciences, P.O. Box 9825, Beijing 100029, China
[b] School of Earth and Environment, University of Leeds, Leeds LS2 9JT, UK

ARTICLE INFO

Article history:
Received 27 June 2013
Accepted 16 March 2014
Available online 29 March 2014

Keywords:
Potassium-rich magmatic rocks
Subduction channel
Enriched asthenospheric mantle source
Plateau uplift
Northwest Tibet

ABSTRACT

Post-collisional potassium-rich mafic magmatism occurred in the northwestern part of the Tibetan Plateau, close to the western syntaxis of the Himalayan orogen, from 8.3 Ma to the present. This magmatism is associated with a tectonic setting influenced by opposing N and S dipping subduction systems formed during the collision of India and Asia. It postdates continent–continent collision and has been linked to the onset of near vertical subduction of Indian continental lithosphere at ~8 Ma. The magmatic rocks have relatively high MgO (4.02–9.04 wt.%), SiO_2 (46.15–57.49 wt.%), K_2O (3.26–7.23 wt.%), Ba (1071–3210 ppm), Th (8.2–85.2 ppm), and Pb (18.6–54.8 ppm) contents, and relatively low Al_2O_3 (12.74–15.78 wt.%). Sr–Nd–Pb isotopic compositions range from: $(^{87}Sr/^{86}Sr)_i$ (0.7072–0.7131), $(^{143}Nd/^{144}Nd)_i$ (0.511953–0.512528) and $(^{206}Pb/^{204}Pb)_i$ (18.67–19.08). Chondrite-normalized rare earth element (REE) patterns are characterized by light REE (LREE) enrichment, flat heavy REE (HREE) patterns and slightly negative Eu anomalies in some of the magmatic rocks. Primitive mantle-normalized incompatible element patterns display strong enrichments in large ion lithophile elements (LILE) relative to high field strength elements (HFSE) and distinct negative Ta–Nb–Ti anomalies. The major and trace element and Sr–Nd–Pb isotope characteristics of the most primitive mafic igneous rocks are interpreted in terms of a mantle source region dominated by subduction channel-derived mélange material derived from both the Indian and Asian subduction systems. This mélange material was underplated below the lithosphere of the Songpan-Ganzi terrane of NW Tibet, probably within the past 25 Ma. Partial melting of the underplated mélange was induced by adiabatic decompression linked to the onset of near vertical subduction of the Indian slab at ~8 Ma.

1. Introduction

Post-collisional potassic magmatism has occurred within the Tibetan Plateau over an extended period from 50 to 8 Ma (e.g. Arnaud et al., 1992; Chen et al., 2010; Chung et al., 2005; Deng, 1998; Ding et al., 2003; Guo et al., 2006, 2013; Roger et al., 2000; Turner et al., 1993, 1996; Wang et al., 2010; Williams et al., 2004; Zhao et al., 2009). Understanding the petrogenesis of this magmatism may provide important constraints on the history and mechanism of Plateau uplift (e.g. Arnaud et al., 1992; Chung et al., 2005; Cooper et al., 2002; Deng, 1998; Ding et al., 2003, 2007; Guo et al., 2006; Mo et al., 2006; Pearce and Mei, 1988; Roger et al., 2000; Turner et al., 1993, 1996; Wang et al., 2008, 2010, 2012; Williams et al., 2004; Zhang et al., 2008). Uplift of the Tibetan Plateau has been linked to a decrease in atmospheric CO_2 concentrations over the past ~40 Myr and to global cooling in Cenozoic times (Dupont-Nivet et al., 2007; Garzione, 2008; Raymo and Ruddiman, 1992).

Potassic magmatic rocks with ages ranging from 8 to 0 Ma (including the only active volcano, Ashi) are mainly limited to the northwestern part of the Plateau, to the east of the western syntaxis of the India-Eurasia collision zone (Fig. 1), which is thought to be one of the most active areas of continental lithospheric subduction and intermediate-depth seismicity in the world (e.g. Negredo et al., 2007). Although there have been previous studies of these post-collisional magmatic rocks (e.g., Arnaud et al., 1992; Cooper et al., 2002; Guo et al., 2006; Turner et al., 1993, 1996; Williams et al., 2004; Zhang et al., 2008), their petrogenesis is still poorly understood. Compared with studies of the post-collisional magmatism in other areas of the Plateau, there is relatively little published geochemical data for the K-rich rocks in northwestern Tibet, because of their inaccessibility and high altitude (more than 4500 m on average). Moreover, most of the previously studied samples were of evolved magmatic rocks, the parental magmas of which have undergone combined crustal contamination and fractional crystallization (AFC; Guo et al., 2006), making it difficult to constrain the nature of their mantle source. The lack of detailed field, petrological

* Corresponding author. Tel.: +86 10 82998393; fax: +86 1062010846.
E-mail address: zfguo@mail.iggcas.ac.cn (Z. Guo).

http://dx.doi.org/10.1016/j.lithos.2014.03.020

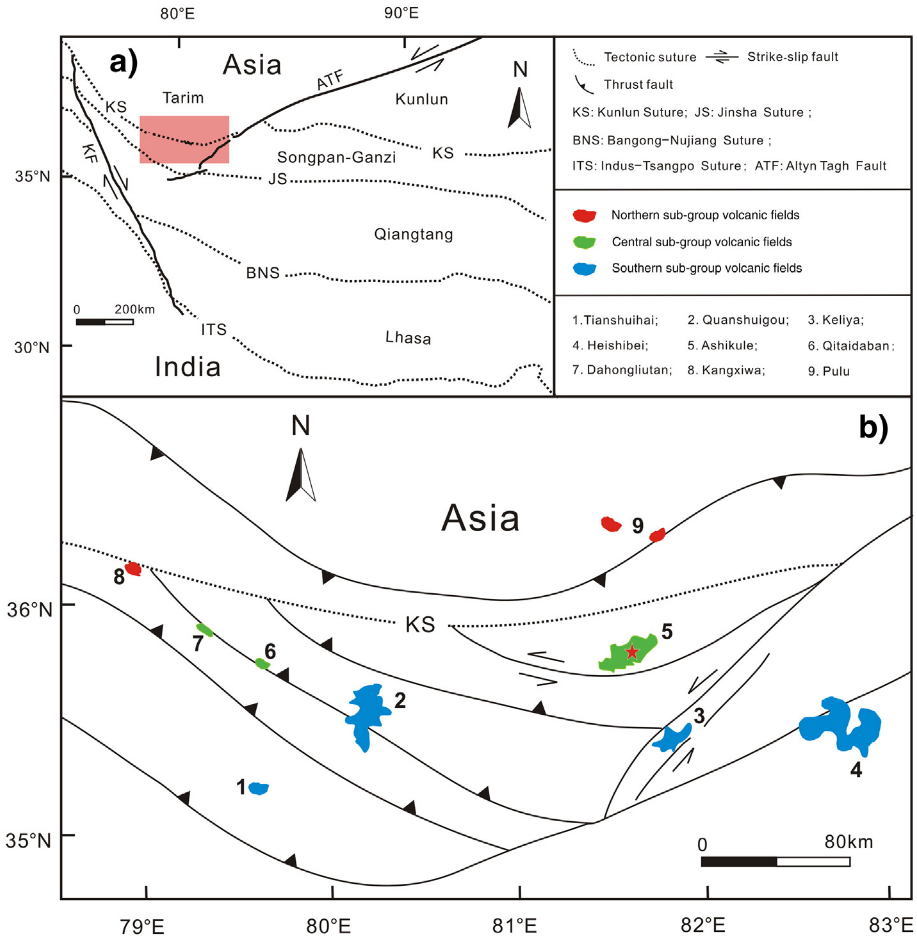

Fig. 1. (a) Regional map showing the position of the study area in relation to the main tectonic sutures in the Tibetan Plateau (modified from Guo et al., 2006). The pink-filled rectangle shows the location of the study area in panel (b). (b) Simplified tectonic map showing the distribution of post-collisional K-rich magmatic rocks in NW Tibet (modified from Guo et al., 2006; Li, 2008). The red star shows the location of the Ashi active volcano in the Ashikule volcanic field, which last erupted in A.D. 1951. (For interpretation of the references to color in this figure legend, the reader is referred to the web version of this article.)

and geochemical data for primitive mafic K-rich volcanic rocks has thus far precluded further constraints on the characteristics of their mantle source region, petrogenesis and geodynamic setting.

This study focuses on a region of post-collisional K-rich mafic magmatism in NW Tibet located between a zone of northward subducting Indian continental lithosphere and southward subducting Asian lithosphere for which the geodynamic setting, though complex, is well constrained by geological and geophysical data (Fig. 2). We report bulk-rock major and trace element and Sr–Nd–Pb isotope data which, combined with previously published geochemical and geophysical data, allow us to develop a robust petrogenetic model for post-collisional magmatism located between converging continental subduction systems.

2. Geological setting

The Tibetan Plateau is a collage of four east–west-trending allochthonous terranes: the Tarim, Songpan-Ganzi, Qiangtang and Lhasa terranes from north to south (Fig. 1a). The post-collisional K-rich magmatic rocks which are the focus of this study are located in the western parts of the Tarim and Songpan-Ganzi terranes in the northwestern Tibetan Plateau, close to the western syntaxis of the India-Eurasia collision zone (Fig. 1). Previous studies (e.g. Negredo et al., 2007) have suggested that the Indian plate continued its northward motion subsequent to India-Asia collision at ~55 Ma (Fig. 2a, b); following inferred slab break-off at ~44–48 Ma Indian continental lithosphere then began to subduct steeply beneath the northwestern part of the Tibetan Plateau from ~8 Ma (Fig. 2c). Geological and geophysical studies (Burtman and Molnar, 1993; Negredo et al., 2007; Searle et al., 2011; Zhao et al., 2010, 2011) indicate a relatively shallow-dipping (~45°) southward subduction of Asian continental lithosphere beneath NW Tibet since ~25 Ma (Fig. 2b, c). The post-collisional K-rich magmatic rocks studied here are thus located between a zone of northward subducting Indian continental lithosphere and southward subducting Asian lithosphere (Fig. 2c).

The age of the magmatism ranges from 8.3 Ma to A.D. 1951 (Supplementary Data Table A.1 and Fig. 3). The magmatic activity is the youngest and highest in the Tibetan Plateau; most of the volcanic fields are located above 4500 m on average (Guo et al., 2006; Liu, 1999). Nine K-rich volcanic fields, including the Ashikule volcanic field in which the only known active volcano Ashi is located (Supplementary Data Table A.1 and Fig. 1), form the basis of this study. They include lava flows, cinder cones, scoria cones, plugs and dykes. Ashi last erupted in A.D. 1951 and has a well-preserved cinder cone and very fresh lava flows (Guo et al., 2006; Liu, 1999). Magmatism is closely associated with a series of strike-slip faults (Fig. 1). Exposures of volcanic rocks range from less than 1 km^2 to 360 km^2. The Dahongliutan and Kangxiwa volcanic fields have the smallest exposed areas of 1–2 km^2, whereas the Quanshuigou and Heishibei volcanic fields have the largest exposed areas of 220–360 km^2. Lava flow thicknesses vary from ~100 m in the Quanshuigou volcanic field to less than 20 m in the Kangxiwa volcanic field. We have sub-divided the volcanic fields into three sub-groups based upon their geochemical characteristics and petrography (Fig. 1): (1) a southern sub-group (including the Tianshuihai, Quanshuigou, Keliya and Heishibei volcanic fields), (2) a central sub-group (including

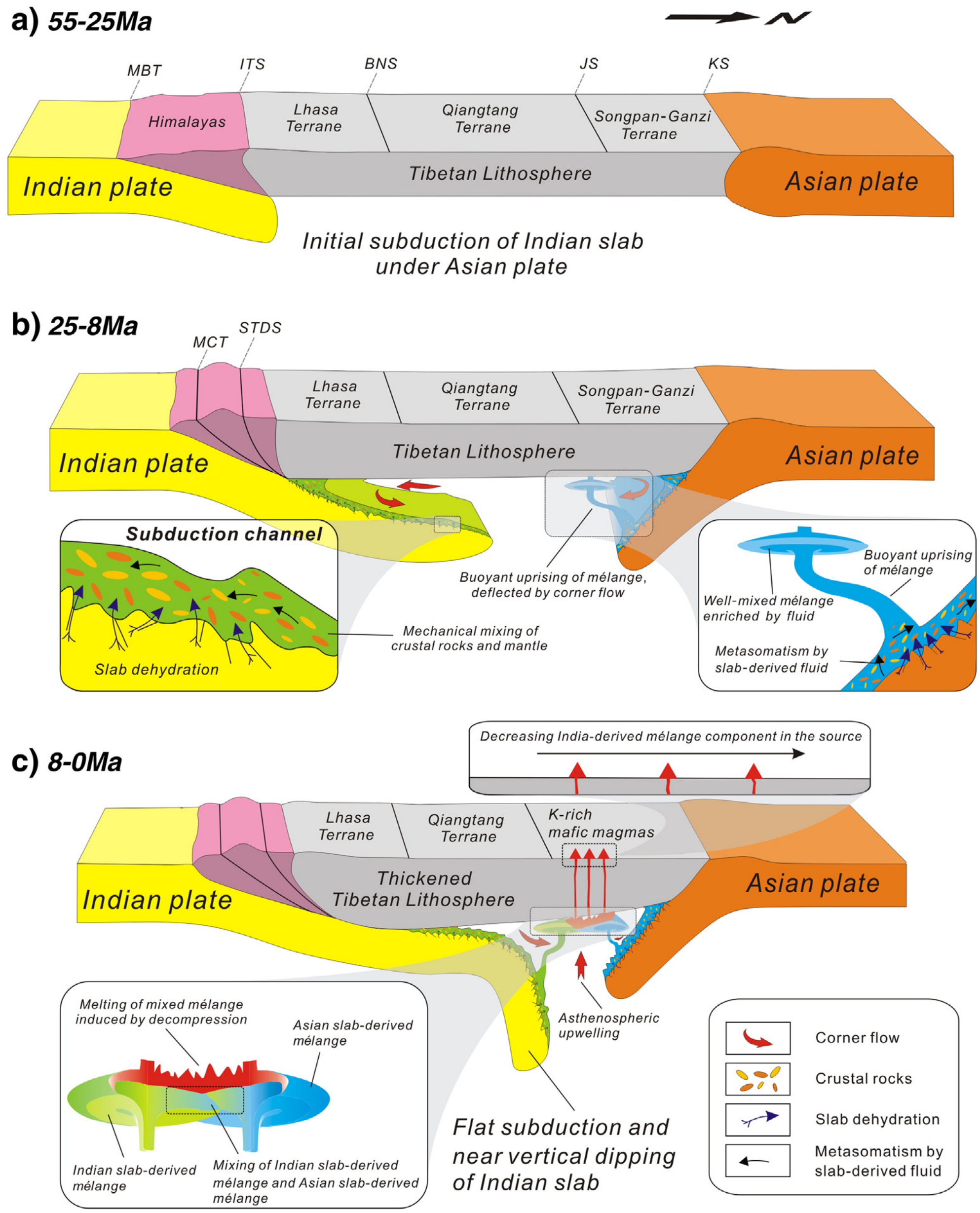

Fig. 2. Geodynamic setting of the post-collisional K-rich magmatism in NW Tibet. The diagram shows a N–S cross section. (a) 55–25 Ma: Northward underthrusting of the Indian plate beneath the Lhasa terrane caused compressional deformation in south Tibet and generation of fluid-metasomatised mélange rocks resulting from dehydration of the subducted Indian slab in a subduction channel during the India–Asia collision from 55 Ma to 25 Ma. (b) 25–8 Ma: Formation of fluid-metasomatised mélange rocks resulting from dehydration of the southward subducted Asian slab in a subduction channel and transportation of the low-density mélange rocks through plumes rising buoyantly from the surface of the subducting Asian slab as a consequence of southward underthrusting of Asian continental lithosphere during the period 25 Ma–8 Ma. The upwelling mélange material is underplated beneath the existing lithosphere of the Songpan-Ganzi terrane. Partial melting of this underplated mélange did not occur because the mantle wedge was too cold and under strong compression due to the opposing northward and southward subduction of the Indian and Asian slabs during this period. The subducted Indian slab continued its northward motion and dehydrated; mechanical mixing of crustal rocks and hydrated mantle occurred in the subduction channel during this period. (c) 8–0 Ma: Generation of the K-rich magmas. The Indian slab began to subduct steeply beneath NW Tibet at ~8 Ma, inducing asthenospheric upwelling as a counter flow. This upwelling caused adiabatic decompression melting of the mixed Indian and Asian mélange material underplating the base of the Tibetan lithosphere. Abbreviations are as follows. MBT: the Main Boundary thrust; MCT: the Main Central thrust; STDS: south Tibetan detachment system; ITS: Indus-Tsangpo Suture; BNS: Bangong-Nujiang Suture; JS: Jinsha Suture; KS: Kunlun Suture. N: north; S: south. Filled red triangles represent the locations of K-rich magmatism in NW Tibet during 8 Ma to the present. (For interpretation of the references to color in this figure legend, the reader is referred to the web version of this article.)

the Ashikule, Qitaidaban and Dahongliutan volcanic fields), and (3) a northern sub-group (including the Kangxiwa and Pulu volcanic fields).

3. Petrography

The studied samples are from small volume dykes, cinder cones, plugs and lava flows (Table 1). They have porphyritic textures with phenocrysts (Fig. 4) of clinopyroxene, phlogopite, amphibole, plagioclase and rare olivine; the groundmass includes phlogopite, clinopyroxene, olivine, sanidine, plagioclase, biotite, amphibole, apatite, Fe–Ti oxides, zircon and glass (Table 1). Phenocrysts are up to 0.2 mm–4 mm in size. All of the analyzed samples are petrographically fresh and show no evidence of significant hydrothermal alteration or weathering.

4. Analytical methods

4.1. Whole rock major and trace element analyses

Samples 4–5 kg in weight were cut into several thin slices. Fresh slices were cleaned three times using deionized water, dried, and then

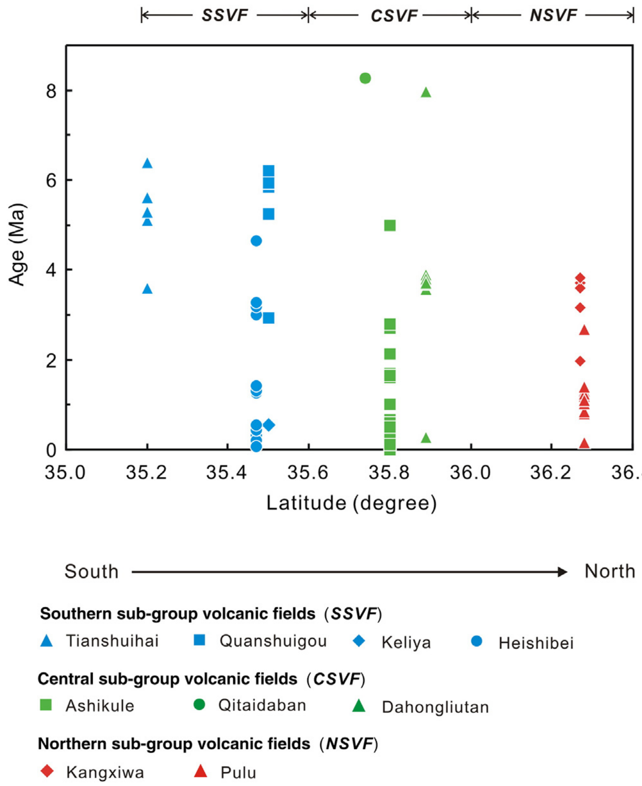

Fig. 3. Age trend of the post-collisional K-rich magmatic rocks from north to south in NW Tibet. The age data are from Supplementary Data Table A.1.

crushed in an agate mortar in preparation for whole-rock major element, trace element and Sr–Nd–Pb isotope analysis.

Whole-rock major element contents (wt%) were determined on fused glass disks by X-ray fluorescence (XRF) using an XRF-1500 sequential spectrometer (SHIMADZU, Japan) at the Institute of Geology and Geophysics, Chinese Academy of Sciences, Beijing (IGGCAS). Sample powders (0.6 g) were fused with $Li_2B_4O_7$ (6 g) in a TR-1000S automatic bead fusion furnace (SHIMADZU, Japan) at 1100 °C for 10 min. Loss on ignition (LOI) was determined by ignition of 2 g whole-rock powder at 1100 °C for 10 h. The analytical precision was better than 2% relative. The detailed analytical procedures follow those reported by Guo et al. (2006). Representative analytical data for the most primitive samples ($SiO_2 < 50$ wt.%; $MgO > 6$ wt.%) are presented in Table 2; the complete data is provided in Supplementary Data Table A.2.

Rare earth element (REE) and trace element contents were analyzed by inductively coupled plasma mass spectrometry (ICP-MS) at IGGCAS using a FINNIGAN MAT II element system. Whole-rock powders (40 mg) were weighted and dissolved in distilled 1 ml HF and 0.5 ml HNO_3 (HNO_3: H_2O = 1:1; in volume ratio) in 7 ml Savillex Teflon screw-cap capsules and then were ultrasonically stirred for 15 min. Subsequently, the solutions were evaporated at 150 °C to dryness and the residue was digested with 1.5 ml HF and 0.5 ml HNO_3 (HNO_3: H_2O = 1:1) in Teflon screw-cap capsules. Then, the solutions were heated at 130 °C initially and at up to 170 °C for 24 h by gradually increasing the temperature during this time. The solutions were then heated at 170 °C for 10 days, dried and redissolved in 2 ml HNO_3 (HNO_3: H_2O = 1:1) in the capsules. The solutions were heated at 150 °C for 5 h and then evaporated, dried and redissolved in 2 ml HNO_3 (HNO_3: H_2O = 1:1) and 2 ml 1% HNO_3 at 150 °C for 5 h in screw-cap capsules in order to ensure that the samples were completely dissolved. The solutions were put into plastic beakers and then 1 ml 500 ppb In was added as an internal standard. Finally, the solutions were diluted in 1% HNO_3 to 50 ml for analysis by ICP-MS. A blank solution was prepared; the total procedural blanks were <50 ng for all the trace elements reported in Table 2 and Supplementary Data Table A.2. During the analytical runs, frequent standard calibrations were performed to correct for instrumental signal drift following the procedure of Guo et al. (2006). Four replicates and two international standards (BHVO-1 and AGV-1) were prepared using the same procedure to monitor the analytical reproducibility. The discrepancy, based on repeated analyses of samples and international standards, is less than 4% for all the trace elements reported. Analyses of the international standards are in excellent agreement with the recommended values (Govindaraju, 1994), and deviate less than 5% from the published values. The detailed analytical procedures follow those of Guo et al. (2005a, 2006).

4.2. Sr–Nd–Pb isotope analyses

Sr–Nd–Pb isotope analyses were performed on a Finnigan MAT262 mass spectrometer at IGGCAS. For Rb–Sr and Sm–Nd isotope analyses, whole-rock chips were ground to 200 mesh (75 μm) in an agate mortar. Whole-rock powders (60 mg) were spiked with mixed isotope tracers (^{87}Rb–^{84}Sr for Rb–Sr isotope analyses and ^{149}Sm–^{150}Nd for Sm–Nd isotope analyses), then dissolved with a mixed acid ($HF:HClO_4 = 3:1$) in Teflon capsules for 7 days at room temperature. Rb and Sr and rare earth element (REE) fractions were separated in solution using AG50W × 8 (H^+) cationic ion-exchange resin columns. Sm and Nd were separated from the other REE fractions in solution using AG50W×8 (H^+) cationic ion-exchange columns and P507 extraction and eluviation resin. The collected Sr and Nd fractions were evaporated and dissolved in 2% HNO_3 to give solutions for analysis by mass spectrometry. The mass fractionation corrections for Sr and Nd isotopic ratios were based on $^{86}Sr/^{88}Sr = 0.1194$ and $^{146}Nd/^{144}Nd = 0.7219$, respectively. The international standard NBS987 gave $^{87}Sr/^{86}Sr$ = 0.710254 ± 16 (n = 8, 2 sigma) (the recommended value is 0.710240) and international standard NBS607 gave $^{87}Sr/^{86}Sr$ = 1.20032 ± 30 (n = 12) (the recommended value is 1.20039). The international La Jolla standard yielded $^{143}Nd/^{144}Nd$ = 0.511862 ± 7 (n = 12) (the recommended value is 0.511859) and international standard BCR-1 yielded $^{143}Nd/^{144}Nd$ = 0.512626 ± 9 (n = 12) (the recommended value is 0.512638). The whole procedure blank is less than 2×10^{-10} g for Rb–Sr isotopic analysis and 5×10^{-11} g for Sm–Nd isotopic analysis. Analytical errors for Sr and Nd isotopic ratios are given as 2 sigma (2σ) in Table 3. The $^{87}Rb/^{86}Sr$ and $^{147}Sm/^{144}Nd$ ratios were calculated using the Rb, Sr, Sm and Nd concentrations obtained by ICP-MS. The initial $^{87}Sr/^{86}Sr$ and $^{143}Nd/^{144}Nd$ ratios were calculated using the average ages of the samples based on $^{40}Ar/^{39}Ar$, K–Ar dating and other analytical methods (Supplementary Data Table A.1).

For whole-rock Pb isotope measurements, in order to minimize contamination from the atmosphere during the crushing process, 100 mesh powders of samples were used. 150 mg whole-rock powder was weighed and dissolved in Teflon capsules using concentrated HF at 120 °C for 7 days. Pb was separated from the silicate matrix and purified using AG1 × 8 anionic ion-exchange columns with dilute HBr as eluant. The whole procedure blank is less than 1 ng. During the period of analysis repeat analyses of the international standard NBS981 yielded $^{204}Pb/^{206}Pb$ = 0.059003 ± 0.000084 (n = 6, 2 sigma) (the certified value is 0.058998), $^{207}Pb/^{206}Pb$ = 0.91449 ± 0.00017 (n = 6) (the certified value is 0.914598), and $^{208}Pb/^{206}Pb$ = 2.16691 ± 0.00097 (n = 6) (the certified value is 2.168099). Pb isotope fractionations were corrected using correction factors based on replicate analyses of the international standard NBS981. The Pb isotope data are reported in Table 4. Detailed sample preparation and analytical procedures for the Sr–Nd–Pb isotope measurements follow those of Guo et al. (2005a, 2006).

5. Results

All of the post-collisional K-rich mafic magmatic rocks studied have relatively high MgO (4.02–9.04 wt.%) contents, Mg-numbers (0.56–

Table 1
Phenocryst and groundmass mineral assemblages of the magmatic rocks in NW Tibet.

Field no.	Sample no.	Field name	Faces	Mg-no.	Phenocrysts	Groundmass
1	CT09	Tianshuihai	Lava flow	0.65	Cpx + Pl + Bi + Fe–Ti	Pl + Sani + Bi + Fe–Ti + G
1	CT12	Tianshuihai	Lava flow	0.65	Pl + Ol + Cpx	Cpx + Sani + Bi + Pl
1	CT17	Tianshuihai	Lava flow	0.64	Cpx + Pl + Bi	Sani + Bi + Fe–Ti + G
1	CT05	Tianshuihai	Lava flow	0.67	Cpx + Pl + Ol	Cpx + Sani + Fe–Ti + G
1	CT23	Tianshuihai	Dyke	0.66	Pl + Phl + Cpx	Pl + Sani + Bi + Fe–Ti
2	QS12	Quanshuigou	Lava flow	0.60	Pl + Cpx + Phl	Phl + Cpx + Sani + Ol + Ap + Pl
2	QS27	Quanshuigou	Lava flow	0.60	Ol + Cpx + Phl	Pl + Cpx + Sani + Bi + G
2	QS19	Quanshuigou	Lava flow	0.59	Cpx + Phl + Pl	Cpx + Sani + Pl + Fe–Ti
2	QS23	Quanshuigou	Lava flow	0.63	Ol + Cpx + Pl + Ap	Cpx + Sani + Pl + Ap + Fe–Ti + G
2	QS18	Quanshuigou	Lava flow	0.63	Ol + Cpx + Pl + Bi	Cpx + Sani + Pl + Fe–Ti
2	QS24	Quanshuigou	Lava flow	0.64	Ol + Cpx + Phl	Pl + Cpx + Sani + Ol + Fe–Ti + G
3	KY03	Keliya	Plug	0.65	Cpx + Ol + Pl + Bi	Cpx + Am + Pl
3	KY02	Keliya	Dyke	0.60	Sani + Pl + Bi + Am	Pl + Cpx + Sani + Fe–Ti
3	KY06	Keliya	Dyke	0.64	Cpx + Pl + Bi	Pl + Bi + Sani + Ap + Qz
3	KY01	Keliya	Lava flow	0.65	Cpx + Pl + Bi + Am	Pl + Sani + Am + Fe–Ti + G
4	HS041	Heishibei	Lava flow	0.59	Cpx + Pl + Ol + Am	Cpx + Pl + Sani + Ol + Fe–Ti
4	HS046	Heishibei	Lava flow	0.56	Cpx + Pl + Am	Pl + Sani + Am + Tit + G
4	HS047	Heishibei	Lava flow	0.57	Cpx + Pl + Ol + Am	Cpx + Pl + Sani + Bi + Ap
4	HS028	Heishibei	Lava flow	0.61	Cpx + Pl + Sani + Fe–Ti	Cpx + Pl + Sani + Am + Fe–Ti
5	AH607	Ashikule	Lava flow	0.63	Cpx + Pl	Cpx + Pl + Sani + Bi + Fe–Ti + G
5	AH605	Ashikule	Lava flow	0.65	Cpx + Pl + Sani + Fe–Ti	Pl + Sani + Bi + Am + G
5	AH609	Ashikule	Plug	0.64	Pl + Bi + Sani + Fe–Ti	Cpx + Pl + Sani + Am
5	AH602	Ashikule	Lava flow	0.68	Cpx + Pl + Phl + Ol	Cpx + Pl + Sani + Ap + G
5	AH618	Ashikule	Lava flow	0.68	Cpx + Pl + Ol + Am	Pl + Sani + Bi + Am + Qz + G
5	AH615	Ashikule	Lava flow	0.68	Cpx + Pl + Phl	Cpx + Pl + Sani + Fe–Ti + Bi + G
7	YS74	Dahongliutan	Lava flow	0.63	Cpx + Pl + Am + Bi	Cpx + Pl + Am + Bi + Sani + Ap + G
7	YS78	Dahongliutan	Lava flow	0.66	Cpx + Pl + Ol + Bi	Pl + Sani + Ol + Cpx + Am + Bi + Zr + G
7	YS05	Dahongliutan	Lava flow	0.63	Pl + Cpx + Am + Ol	Pl + Sani + Cpx + Am + Bi + Fe–Ti
7	YS79	Dahongliutan	Lava flow	0.62	Cpx + Ol + Bi + Am + Fe–Ti	Cpx + Pl + Sani + Am + Bi + Fe–Ti
7	YS07	Dahongliutan	Lava flow	0.62	Cpx + Pl + Am + Ol + Bi	Cpx + Ol + Pl + Bi + Am + G
8	KX44	Kangxiwa	Lava flow	0.71	Cpx + Pl + Bi + Ol	Cpx + Pl + Ap + Fe–Ti + G
8	KX51	Kangxiwa	Lava flow	0.69	Cpx + Pl + Ol + Ap	Cpx + Pl + Ap + Fe–Ti + G
8	KX80	Kangxiwa	Lava flow	0.70	Cpx + Pl + Ol + Am	Cpx + Pl + Ap + Fe–Ti + Bi + G
8	KX49	Kangxiwa	Lava flow	0.70	Cpx + Pl + Ol + Bi	Cpx + Pl + Ap + Fe–Ti
8	KX62	Kangxiwa	Lava flow	0.70	Cpx + Pl + Ol	Cpx + Pl + Ap + Zr + G
9	PL53	Pulu	Lava flow	0.68	Ol + Cpx + Pl + Bi	Pl + Sani + Cpx + Bi + Fe–Ti
9	PL61	Pulu	Lava flow	0.68	Ol + Cpx + Pl	Pl + Sani + Cpx + Bi
9	PL3	Pulu	Lava flow	0.56	Ol + Cpx + Pl + Bi	Pl + Sani + Bi + Fe–Ti
9	PL18	Pulu	Lava flow	0.59	Ol + Cpx + Pl	Pl + Cpx + Bi + Fe–Ti
9	PL92	Pulu	Lava flow	0.59	Ol + Cpx + Pl	Cpx + Ol + Pl + G
9	PL43	Pulu	Lava flow	0.59	Ol + Cpx + Pl + Fe–Ti	Cpx + Ol + Pl + Zr + Fe–Ti + G

Field no. refers to number of the volcanic field in Fig. 1. Field name corresponds to that in Fig. 1.
Am: amphibole; Ap: apatite; Bi: biotite; Cpx: clinopyroxene; Fe–Ti: Fe–Ti oxides; G: glass; Ol: olivine; Phl: phlogopite; Pl: plagioclase; Sani: sanidine; Tit: titanite; Zr: zircon.

0.71), Ni (87–340 ppm) and Cr (91–408 ppm) contents (Table 2; Supplementary Data Table A.2), suggesting primitive characteristics. Most of the studied samples are potassic, with K_2O/Na_2O ratios ranging from 1 to 2. Their compositions in an $Na_2O + K_2O$ vs SiO_2 classification diagram lie almost totally within the trachybasalt–basaltic trachyandesite–trachyandesite–tephrite–phonotephrite–tephriphonolite fields (Fig. 5a). A plot of K_2O vs SiO_2 shows that the studied samples plot in the shoshonitic field (Fig. 5b). Based on the results of previous studies (e.g. Guo et al., 2006), combined assimilation and fractional crystallization (AFC) processes have modified the compositions of the primary magmas, resulting in a range of evolved magma compositions with MgO < 6wt.%. The dispersion of compositions in Fig. 5 is indicative of the effects of AFC processes (cf., Guo et al., 2006). The most primitive samples (MgO > 6 wt.%) from this study are CT12, CT17, CT23, QS27, QS19, QS23, QS18, QS24, KY06, AH607, AH605, AH609, AH602, AH618, AH615, YS05, KX44, KX51, KX80, KX49, KX62, PL53, and PL61 (Supplementary Data Table A.2; Table 2). These are highlighted in Fig. 5 and provide the main focus for subsequent discussion.

The K-rich magmatic rocks have enriched light REE (LREE) and relatively flat heavy REE (HREE) patterns; slightly negative Eu anomalies are evident in the REE patterns for the southern volcanic fields (Fig. 6). Primitive mantle-normalized incompatible trace element patterns (Fig. 7) are characterized by distinct negative Nb–Ta–Ti anomalies and positive anomalies in the large ion lithophile elements (LILE) (e.g. Ba, Th), and Pb, typical of subduction-related magmatic rocks.

In detail, the concentrations of LILE (Ba, Rb), Pb and LREE (La, Ce) are higher in the central subgroup than those in the northern and southern subgroups (Fig. 7). Th contents decrease from the southern subgroup through the central subgroup to the northern subgroup. REE patterns are steeper in the central subgroup than those in the northern and southern subgroups (Fig. 6). The average value of La/Yb is 82.8, 76.2, 55.8 in the central, northern and southern subgroups, respectively (Supplementary Data Table A.2; Table 2). Ba/Th increases and Th/Nd decreases from the southern through the central to the northern subgroup (Fig. 8).

The NW Tibetan post-collisional magmatic rocks have high $(^{87}Sr/^{86}Sr)_i$ (0.7072–0.7131) and low $(^{143}Nd/^{144}Nd)_i$ (0.511953–0.512528) relative to Bulk Silicate Earth (BSE) values, and high $(^{207}Pb/^{204}Pb)_i$ (15.57–15.95) and $(^{208}Pb/^{204}Pb)_i$ (38.66–39.58) at relatively constant $(^{206}Pb/^{204}Pb)_i$ (18.67–19.08) with respect to the Northern Hemisphere Reference Line (NHRL) (Tables 3 and 4; Fig. 9). $(^{87}Sr/^{86}Sr)_i$ varies considerably in the southern subgroup but is relatively constant in the northern subgroup (Figs. 8b and 9). The Sr–Nd isotope compositions (Fig. 9) plot within a triangular field bounded by the isotopic compositions of depleted MORB-source mantle (DMM), Indian continental basement [proxied by the isotopic composition of the Higher Himalayan Crystalline Series; see Pan et al. (2004) and Richards et al. (2005) and references therein for a more detailed discussion] and Asian continental basement [proxied by the isotopic composition of deep-drill-core metamorphic rock samples from the basement of the central Tarim Basin to

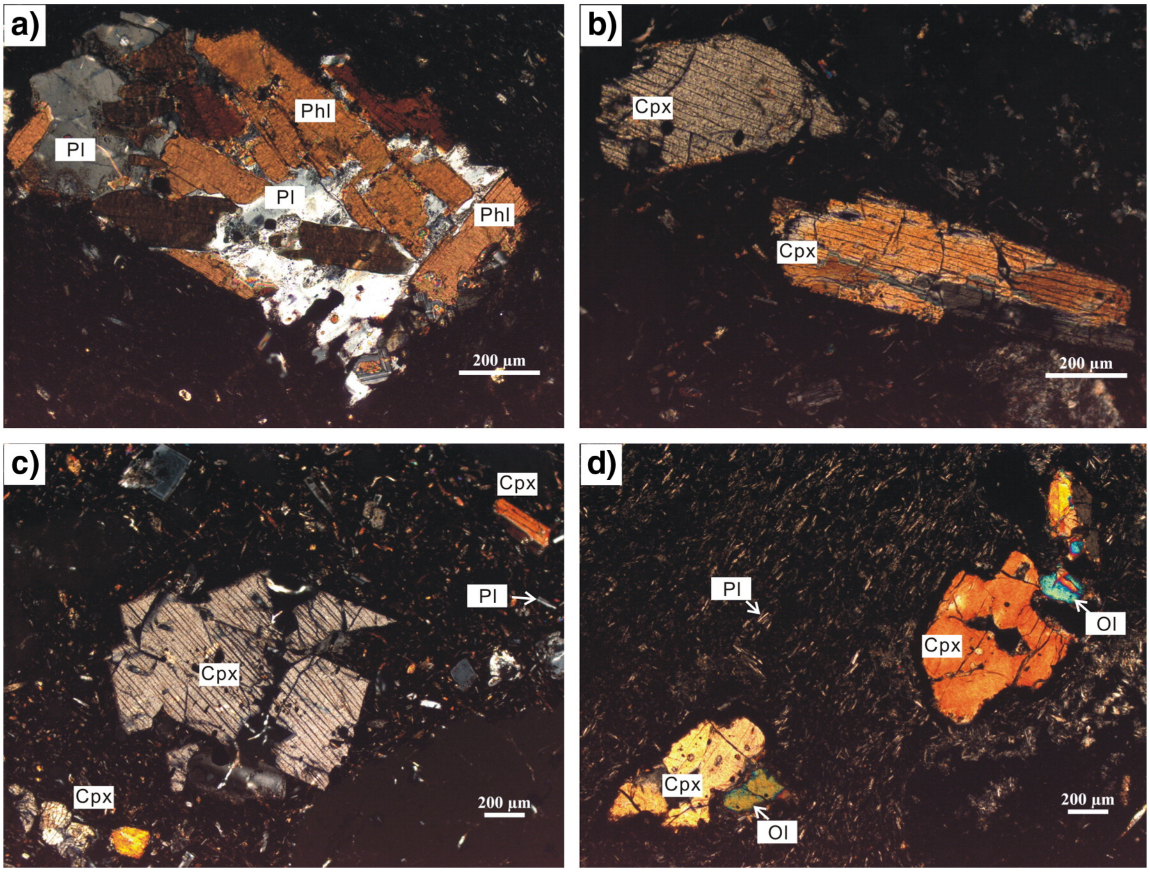

Fig. 4. Representative photomicrographs in K-rich volcanic rocks in NW Tibet (cross-polarized light). (a) A glomeroporphyritic aggregate of phlogopite and plagioclase in sample (AH615) from the Ashikule volcanic field; (b,c) porphyritic textures with phenocrysts of clinopyroxene in sample (QS12) of the Quanshuigou volcanic field; (d) porphyritic texture with phenocrysts of clinopyroxene and microphenocrysts of olivine in sample (HS041) from the Heishibei volcanic field. Cpx, clinopyroxene; Ol, olivine; Phl, phlogopite; Pl, plagioclase.

the north of the Tibetan Plateau (Fig. 1); see Jiang et al. (2004), Zhang et al. (2004), Guo et al. (2005b) and Zhang et al. (2009) and references therein for a more detailed discussion].

6. Discussion

The post-collisional K-rich magmatism of the Tibetan Plateau has been considered to be important in constraining the uplift history of the Plateau (e.g. Arnaud et al., 1992; Chen et al., 2010; Chung et al., 2005; Ding et al., 2007; Guo et al., 2006; Pearce and Mei, 1988; Roger et al., 2000; Turner et al., 1993, 1996; Wang et al., 2012; Williams et al., 2001, 2004). The major and trace element contents and Sr–Nd–Pb isotope compositions of the most primitive mafic rocks provide important insights on nature of their mantle source, and the geodynamic setting, whilst their ages can constrain the timing of Plateau uplift.

6.1. Age trend of the K-rich magmatism in NW Tibet

To constrain the age relationships of the potassium-rich magmatism in NW Tibet (Fig. 1), we have compiled all the available geochronological data from the published literature (Supplementary Data Table A.1). Several different methods (e.g. $^{40}Ar/^{39}Ar$, K–Ar, Zircon U–Pb) have been used to date the magmatic rocks. We have checked the data quality and compared the ages from the different methods to constrain the age ranges of the magmatic rocks. These data indicate that age of the magmatism ranges from 8 Ma to the present day; the history of volcanism appears to be longer in the central subgroup volcanic fields than those in the southern and northern sub groups (Fig. 3). The unique active volcano in the Plateau, Ashi, is located within the central subgroup (Fig. 1).

6.2. Nature of the mantle source region of the K-rich magmas

The post-collisional K-rich mafic magmatic rocks are characterized by significant enrichment in LILE and LREE relative to HFSE and HREE, with strongly negative Nb–Ta–Ti anomalies and positive Pb anomalies in primitive mantle — normalized incompatible trace element patterns (Fig. 7), consistent with an origin as subduction-related magmas (e.g. Gill, 1981; Pearce and Parkinson, 1993). Their Sr–Nd–Pb isotope compositions fall within a field enclosed by depleted MORB-source mantle (Workman and Hart, 2005), Indian continental basement and Asian continental basement (Fig. 9), suggesting that their source region contains both India- and Asia-derived continental crustal components. Evidence for opposing northward subduction of the Indian slab (e.g. Li, 2008; Zhao et al., 2010) and southward subduction of Asian lithosphere beneath NW Tibet (e.g. Negredo et al., 2007; Zhao et al., 2011) supports this inference.

Marschall and Schumacher (2012) proposed a physical process by which components from a subducting slab and overlying mantle wedge can be transported into the mantle source of subduction-related magmas. This involves formation of a mélange zone within a subduction channel on the top surface of the slab in which hydrated mantle rocks are mixed with material derived from the subducting slab, including trench sediments (cf., Gerya et al., 2002; Guillot et al., 2009). The trace-element characteristics of exhumed metamorphic mélange rocks are similar to those of subduction-related magmas (Marschall and Schumacher, 2012), with the distinctive enrichment in LILE and significant depletion in HFSE (e.g. Nb, Ta and Ti), suggesting that deeply subducted mélange components may provide an important source component for arc magmas. We have developed this model for the NW Tibetan post-collisional tectonic setting (Fig. 2), proposing the

Table 2
Major and trace element analyses of the representative potassium-rich magmatic rocks in NW Tibet.

Field no.:	2	2	2	2	2	5	5	5	5
Sample no.:	QS27	QS19	QS23	QS18	QS24	AH607	AH605	AH609	AH602
Field name:	Quanshuigou	Quanshuigou	Quanshuigou	Quanshuigou	Quanshuigou	Ashikule	Ashikule	Ashikule	Ashikule
Age (Ma):	5.23	5.23	5.23	5.23	5.23	1.07	1.07	1.07	1.07
SiO_2	48.80	49.66	47.97	48.75	49.62	47.90	46.15	48.12	47.11
TiO_2	1.50	1.40	1.58	1.67	1.72	1.90	2.39	1.93	2.51
Al_2O_3	13.88	13.27	14.61	14.75	14.95	13.91	13.78	14.24	14.10
TFe_2O_3[a]	10.86	10.77	10.33	10.45	10.09	10.79	11.43	9.61	9.99
MnO	0.12	0.13	0.13	0.11	0.12	0.18	0.16	0.14	0.15
MgO	6.49	6.23	7.09	7.33	7.16	7.31	8.52	6.85	8.46
CaO	9.84	9.58	9.10	8.75	8.38	9.21	8.28	10.21	8.68
Na_2O	3.38	3.21	3.30	3.48	3.03	3.53	3.49	3.26	3.32
K_2O	3.86	4.30	4.64	3.72	3.80	4.35	4.74	4.45	4.41
P_2O_5	1.26	1.44	1.25	0.99	1.12	0.93	1.06	1.19	1.25
LOI	1.01	1.34	0.76	0.59	1.32	0.82	1.57	0.68	0.66
Mg-no.	0.60	0.59	0.63	0.63	0.64	0.63	0.65	0.64	0.68
La	113.7	104.3	101.4	92.5	71.8	137.7	97.3	95.8	116.2
Ce	247.9	203.2	221.7	191.7	152.2	312.8	174.2	197.4	217.8
Pr	29.8	23.7	26.9	23.8	20.6	37.2	19.5	24.1	22.4
Nd	101.7	78.3	77.2	79.4	69.3	126.1	60.8	86.9	86.5
Sm	19.5	18.6	14.3	15.6	10.9	18.9	13.6	14.6	14.9
Eu	4.14	3.31	3.74	3.31	2.71	4.73	3.37	4.22	4.13
Gd	15.43	14.16	15.29	13.74	11.68	13.57	7.85	11.87	11.28
Tb	1.65	1.47	1.68	1.42	1.29	1.36	0.84	1.59	1.37
Dy	5.78	6.11	8.12	7.11	6.18	5.84	4.79	6.32	5.63
Ho	0.96	1.14	1.27	1.15	1.02	0.95	0.99	1.06	0.97
Er	2.43	2.62	2.85	2.73	2.52	2.38	2.95	2.29	2.48
Tm	0.33	0.39	0.37	0.35	0.31	0.32	0.41	0.34	0.29
Yb	1.87	2.12	2.11	1.96	1.76	1.86	2.63	1.78	1.69
Lu	0.25	0.31	0.28	0.28	0.26	0.33	0.38	0.31	0.26
Sc	25.6	23.8	22.1	18.9	22.7	24.2	23.7	17.9	27.6
V	172.4	169.5	201.7	179.1	182.6	162.3	234.9	136.2	157.8
Cr	251.8	236.7	352.6	338.1	369.5	171.6	205.1	175.9	172.3
Co	37.3	33.9	36.2	29.7	34.1	39.4	32.8	27.5	31.7
Ni	143.3	162.2	135.8	152.9	147.6	115.3	109.7	93.6	98.4
Cu	26.8	32.3	32.6	28.3	25.4	35.8	37.6	33.1	42.5
Zn	127.5	132.3	159.3	141.8	146.2	117.4	125	109.2	114.3
Ga	20.5	19.3	18.6	23.7	21.9	23.7	21.6	18.5	20.4
Rb	114.2	127.5	119.3	108.6	126.2	98.5	113.2	99.6	109.2
Sr	1731	1647	1718	1752	1678	1376	1528	1406	1390
Y	31	28.6	23.5	28.7	31.6	19.4	23.6	21.7	20.8
Zr	362	417	393	368	401	317	289	351	324
Nb	35.7	33.9	30.8	29.4	37.4	55.9	48.3	52.4	46.1
Ba	2374	2736	2696	2520	2189	1675	2003	1948	1896
Hf	10.9	13.2	11.7	9.6	8.3	10.6	8.5	9.7	11.5
Ta	2.14	1.28	1.31	2.81	1.77	3.18	2.64	3.32	3.56
Pb	24	23.8	31.2	27.3	25.4	37.4	41.9	26.8	34.1
Th	37.5	85.2	81.8	42.5	53.9	15.1	16.6	15.3	14.8
U	4.19	4.25	6.34	3.14	2.36	3.79	3.71	3.89	3.86

Field no.:	5	5	8	8	8	8	8	9
Sample no.:	AH618	AH615	KX44	KX51	KX80	KX49	KX62	PL61
Field name:	Ashikule	Ashikule	Kangxiwa	Kangxiwa	Kangxiwa	Kangxiwa	Kangxiwa	Pulu
Age (Ma):	1.07	1.07	3.24	3.24	3.24	3.24	3.24	1.20
SiO_2	46.73	47.40	48.75	48.62	49.47	48.52	48.55	49.52
TiO_2	2.38	2.17	1.90	1.54	1.48	1.86	1.91	1.83
Al_2O_3	13.85	14.55	12.76	13.55	13.71	12.79	12.74	13.43
TFe_2O_3[a]	10.23	10.37	9.12	9.30	9.00	9.15	9.23	9.50
MnO	0.16	0.17	0.15	0.12	0.13	0.14	0.15	0.11
MgO	8.76	9.04	8.83	8.25	8.29	8.77	8.83	8.10
CaO	8.43	7.27	8.08	8.91	9.32	8.56	8.52	8.51
Na_2O	3.76	3.44	2.89	3.64	2.49	2.90	3.48	3.17
K_2O	4.74	4.52	5.71	4.68	4.86	5.77	5.31	4.89
P_2O_5	0.96	1.06	1.80	1.39	1.26	1.54	1.28	0.94
LOI	1.79	2.05	0.74	1.46	1.13	0.71	0.86	1.08
Mg-no.	0.68	0.68	0.71	0.69	0.70	0.70	0.70	0.68
La	105.9	103.6	117.8	132.3	131.8	115.3	136.2	172.8
Ce	192.6	204.2	251.3	241.6	247.2	248.6	281.5	342.6
Pr	21.3	23.7	30.7	29	31.5	31.4	34.9	35.7
Nd	73.8	92.3	122.5	95.4	114.7	125.3	121.6	109.5
Sm	12.3	15.1	28.1	19.6	21.8	29.3	23.8	20.2
Eu	2.94	4.09	6.53	4.02	5.81	6.46	4.83	5.13
Gd	9.02	12.68	17.2	7.31	15.26	17.11	12.29	14.66

Table 2 (*continued*)

Field no.:	5	5	8	8	8	8	8	9
Sample no.:	AH618	AH615	KX44	KX51	KX80	KX49	KX62	PL61
Field name:	Ashikule	Ashikule	Kangxiwa	Kangxiwa	Kangxiwa	Kangxiwa	Kangxiwa	Pulu
Age (Ma):	1.07	1.07	3.24	3.24	3.24	3.24	3.24	1.20
Tb	1.08	1.57	2.08	0.94	1.76	2.03	1.45	1.72
Dy	4.83	6.39	8.22	4.79	7.32	8.75	6.63	7.14
Ho	0.94	1.01	1.34	0.88	1.1	1.51	1.28	1.02
Er	2.45	2.56	3.17	1.96	2.38	3.25	2.69	2.45
Tm	0.33	0.37	0.36	0.29	0.31	0.38	0.35	0.28
Yb	1.72	1.91	2.19	1.98	1.89	1.92	1.79	1.66
Lu	0.24	0.35	0.33	0.28	0.31	0.24	0.3	0.21
Sc	24.4	28.3	23.5	30.7	28.1	23.6	29.3	25.7
V	215.3	190.6	231.7	262.3	251.4	250.7	254.5	162.3
Cr	169.8	229.5	306.7	393.2	378.4	283.1	339.7	408.2
Co	41.3	35.2	32.9	40.5	38.9	31.3	36.5	51.8
Ni	104.5	113.8	183.5	148.3	152.8	173.6	168.2	295.3
Cu	39.7	38.3	39.6	36.8	35.1	40.8	36.4	34.8
Zn	105.5	132.6	156.2	201.3	208.5	141.4	219.8	131.4
Ga	21.9	21.3	18.3	21.1	21.6	19	22.3	18.6
Rb	104.5	110.6	263.3	241.7	238.8	269.1	166.4	87.5
Sr	1471	1428	1921	1729	1803	1846	1783	1134
Y	22.4	21.3	28.4	32.5	33.6	31.7	28.3	27.1
Zr	305	326	536	520	516	472	418	482
Nb	49.6	53.2	37.2	27.9	28.4	40.6	33.9	36.3
Ba	2101	2014	2451	2687	2715	2369	2361	1246
Hf	10.2	8.9	13.2	12.6	11.8	14.1	12.8	17.9
Ta	2.69	3.93	2.35	1.13	1.25	2.17	1.26	1.18
Pb	31.7	41	27.7	23.4	27.9	30.6	35.1	47.4
Th	15.7	13.9	13.2	8.2	10.6	14.2	12.9	15.1
U	4.11	3.46	3.26	4.72	3.35	4.61	5.18	5.36

Major element oxide contents are normalized to 100 wt.% on a volatile-free basis. Field no. refers to number of the volcanic field in Fig. 1. Age (Ma) is the average value of the ages of the volcanic fields calculated from all of age data shown in Supplementary Data Table A.1. Mg-no. = Mg/(Mg + Fe^{2+}), calculated assuming Fe_2O_3/(FeO + Fe_2O_3) = 0.20.

[a] Total iron is given as Fe_2O_3.

involvement of isotopically distinct Indian and Asian mélange components in the petrogenesis of the K-rich magmas.

Enrichment of the source of subduction-related magmas has traditionally been attributed to migration of aqueous fluids and/or melts derived from the subducted slab into the mantle wedge (e.g. Elburg et al., 2002; Gill, 1981; Guo et al., 2013; Hawkesworth et al., 1997; Johnson and Plank, 1999; Pearce, 1983). Compositional distinctions have been identified between subduction-related magmatic rocks whose sources have been modified by subduction-related fluids and those that have been enriched by slab-derived melts (e.g. Class et al., 2000; Guo et al., 2013; Hawkesworth et al., 1997; Johnson and Plank, 1999; Tatsumi et al., 1986; Woodhead et al., 2001). Slab-derived fluids, which carry little REE and HFSE, can introduce significant amounts of LILE (e.g. K, Rb, Cs, Sr, Ba, U, Pb) from the subducting slab to the source region in the mantle wedge, whilst slab-derived melts are characterized by high Th and LREE concentrations. On the basis of the above discussion, the northward changes in REE and LILE (Figs. 6–8) of the K-rich rocks could be simply explained by influx of Indian slab-derived melts and Asian slab-derived fluids to the mantle source of the magmas in the southern and northern subgroups, respectively. Recent studies (e.g. Prelević et al., 2013; Tommasini et al., 2011) have, however, suggested that Th (and Sm) enrichments in K-rich magmatic rocks could be linked to the presence of subducted blueschist-facies mélange components in their mantle source. Zoisite/epidote and lawsonite in blueschists are thought to be major repositories of Sr, Pb, U, Th, and LREE (Brunsmann et al., 2000; Feineman et al., 2007; Frei et al., 2004; Hickmott et al., 1992; Spandler et al., 2003; Tommasini et al., 2011; Usui et al., 2006) because of their high partition coefficients for these elements. Partial melting of well-mixed blueschist-facies mélange rocks within the mantle wedge could thus result in Th enrichment of subduction-related magmas.

The potassic magmatic rocks from NW Tibet studied here have variable Th and Sm enrichments with respect to La (Fig. 8c). They define two near linear trends in a $(^{87}Sr/^{86}Sr)_i$ vs Ba/Th diagram (Fig. 8b); one trend lies between a depleted mantle source component and an inferred Asian mélange component with high Ba/Th and the other between the same depleted mantle and an inferred Indian mélange component with low Ba/Th. The variation of $(^{87}Sr/^{86}Sr)_i$ vs Ba/Th thus suggests that the mantle source of the Tibetan potassic magmas consist of three end-members: (1) a depleted MORB-source mantle (cf., Workman and Hart, 2005), (2) an Asian mélange component which has $(^{87}Sr/^{86}Sr)_i$ of ~0.708 and (3) an Indian mélange component with $(^{87}Sr/^{86}Sr)_i$ >0.713 and Ba/Th similar to Indian continental basement. This suggests that the Indian and Asian subducted mélanges provide important source components for the K-rich magmas in the southern and northern subgroups, respectively (Fig. 8b).

6.3. A petrogenetic model for the K-rich magmatic rocks in NW Tibet

The most primitive post-collisional K-rich mafic magmatic rocks which form the basis of this study have high MgO contents, Mg-numbers and Ni concentrations (Table 2; Supplementary Data Table A.2), indicating that they are partial melting products of the upper mantle. Their ages (8.3 Ma–present) reflect an important tectono-magmatic event which induced partial melting of the upper mantle beneath NW Tibet. This event can be linked to the onset of near vertical subduction of Indian continental lithosphere at ~8 Ma (e.g., Negredo et al., 2007; Zhao et al., 2010, 2011).

Marschall and Schumacher (2012) provide an elegant physico-chemical conceptual framework for subduction zones that involves subduction channel mélanges in the recycling of trench sediments into the source of subduction-related magmas. We have adapted this model for the NW Tibetan geodynamic setting of converging subduction systems and propose a two-stage petrogenetic model for the post-collisional K-rich magmatism. The first stage involves formation of mélanges in the Asian and Indian subduction channels at the slab–mantle interface

Table 3
Sr and Nd isotope compositions of the post-collisional potassium-rich magmatic rocks in NW Tibet.

Field no.	Sample no.	Field name	$^{87}Rb/^{86}Sr$	$^{87}Sr/^{86}Sr \pm 2\sigma$	$(^{87}Sr/^{86}Sr)_i$	εSr(i)	$^{147}Sm/^{144}Nd$	$^{143}Nd/^{144}Nd \pm 2\sigma$	$(^{143}Nd/^{144}Nd)_i$	εNd(i)
1	CT09	Tianshuihai	0.1914	0.708172 ± 12	0.708158	52.01	0.0830	0.512335 ± 7	0.512332	−5.84
1	CT12	Tianshuihai	0.1719	0.711863 ± 11	0.711850	104.42	0.1110	0.512241 ± 6	0.512237	−7.69
1	CT17	Tianshuihai	0.2245	0.708194 ± 15	0.708177	52.29	0.1129	0.512305 ± 9	0.512301	−6.44
1	CT05	Tianshuihai	0.2275	0.707962 ± 14	0.707945	48.99	0.1076	0.512218 ± 8	0.512214	−8.13
1	CT23	Tianshuihai	0.2460	0.707685 ± 13	0.707667	45.04	0.0919	0.512441 ± 5	0.512438	−3.77
2	QS12	Quanshuigou	0.1898	0.707816 ± 17	0.707802	46.96	0.0947	0.512156 ± 6	0.512153	−9.33
2	QS27	Quanshuigou	0.1909	0.708529 ± 14	0.708515	57.08	0.1159	0.512341 ± 8	0.512337	−5.74
2	QS19	Quanshuigou	0.2241	0.712843 ± 15	0.712826	118.28	0.1436	0.512167 ± 10	0.512162	−9.15
2	QS23	Quanshuigou	0.2010	0.713148 ± 12	0.713133	122.63	0.1120	0.512328 ± 8	0.512324	−5.99
2	QS18	Quanshuigou	0.1794	0.709648 ± 10	0.709635	72.97	0.1188	0.512236 ± 7	0.512232	−7.79
2	QS24	Quanshuigou	0.2177	0.710213 ± 9	0.710197	80.95	0.0951	0.512148 ± 9	0.512145	−9.49
3	KY03	Keliya	0.1866	0.708454 ± 11	0.708453	56.11	0.1228	0.512207 ± 6	0.512207	−8.40
3	KY02	Keliya	0.1655	0.709312 ± 17	0.709311	68.29	0.1426	0.512316 ± 10	0.512315	−6.28
3	KY06	Keliya	0.1310	0.709471 ± 15	0.709470	70.56	0.1154	0.512127 ± 7	0.512127	−9.96
3	KY01	Keliya	0.1590	0.708103 ± 16	0.708102	51.13	0.1294	0.512249 ± 6	0.512249	−7.58
4	HS041	Heishibei	0.3029	0.707849 ± 18	0.707841	47.46	0.1207	0.512258 ± 11	0.512257	−7.40
4	HS046	Heishibei	0.3350	0.710381 ± 12	0.710373	83.39	0.1226	0.512105 ± 9	0.512104	−10.38
4	HS047	Heishibei	0.2795	0.709417 ± 10	0.709410	69.72	0.1152	0.512263 ± 8	0.512262	−7.30
4	HS028	Heishibei	0.3416	0.710824 ± 15	0.710815	89.67	0.1247	0.512237 ± 10	0.512236	−7.81
5	AH607	Ashikule	0.2071	0.709036 ± 16	0.709033	64.36	0.0906	0.512387 ± 6	0.512386	−4.88
5	AH605	Ashikule	0.2144	0.709531 ± 15	0.709528	71.38	0.1353	0.512129 ± 9	0.512128	−9.92
5	AH609	Ashikule	0.2050	0.707619 ± 17	0.707616	44.25	0.1016	0.512483 ± 8	0.512482	−3.01
5	AH602	Ashikule	0.2273	0.707319 ± 12	0.707316	39.98	0.1042	0.512474 ± 10	0.512473	−3.19
5	AH618	Ashikule	0.2056	0.709224 ± 15	0.709221	67.03	0.1008	0.512116 ± 7	0.512115	−10.17
5	AH615	Ashikule	0.2241	0.710308 ± 14	0.710305	82.42	0.0989	0.512402 ± 7	0.512401	−4.59
7	YS74	Dahongliutan	0.5182	0.710016 ± 12	0.709988	77.96	0.1033	0.512287 ± 6	0.512284	−6.80
7	YS78	Dahongliutan	0.4278	0.707924 ± 13	0.707901	48.34	0.1138	0.512395 ± 8	0.512392	−4.70
7	YS05	Dahongliutan	0.4048	0.707637 ± 16	0.707615	44.28	0.1181	0.512412 ± 9	0.512409	−4.37
7	YS79	Dahongliutan	0.2959	0.708453 ± 10	0.708437	55.95	0.1108	0.512462 ± 9	0.512459	−3.39
7	YS07	Dahongliutan	0.2610	0.708134 ± 17	0.708120	51.45	0.1058	0.512395 ± 7	0.512392	−4.70
8	KX44	Kangxiwa	0.3966	0.708143 ± 18	0.708125	51.51	0.1387	0.512179 ± 10	0.512176	−8.93
8	KX51	Kangxiwa	0.4045	0.708247 ± 11	0.708228	52.98	0.1242	0.512062 ± 9	0.512059	−11.21
8	KX80	Kangxiwa	0.3832	0.707967 ± 16	0.707949	49.02	0.1149	0.512148 ± 11	0.512146	−9.52
8	KX49	Kangxiwa	0.4218	0.708645 ± 13	0.708626	58.62	0.1414	0.512097 ± 12	0.512094	−10.53
8	KX62	Kangxiwa	0.2700	0.708317 ± 12	0.708305	54.06	0.1183	0.512124 ± 8	0.512121	−9.99
9	PL53	Pulu	0.2432	0.708761 ± 17	0.708757	60.44	0.0994	0.512179 ± 7	0.512178	−8.94
9	PL61	Pulu	0.2233	0.708827 ± 14	0.708823	61.39	0.1115	0.512053 ± 8	0.512052	−11.40
9	PL3	Pulu	0.3380	0.708562 ± 10	0.708556	57.60	0.1085	0.512427 ± 10	0.512426	−4.10
9	PL18	Pulu	0.2130	0.708004 ± 12	0.708000	49.71	0.0980	0.512013 ± 11	0.512012	−12.18
9	PL92	Pulu	0.2359	0.708951 ± 11	0.708947	63.14	0.1128	0.512338 ± 6	0.512337	−5.84
9	PL43	Pulu	0.3353	0.708845 ± 13	0.708839	61.61	0.1014	0.512309 ± 7	0.512308	−6.40

Field no. refers to number of volcanic field in Fig. 1. Chondritic uniform reservoir (CHUR) at the present day [$(^{87}Rb/^{86}Sr)_{CHUR} = 0.0847$ (McCulloch and Black, 1984); $(^{87}Sr/^{86}Sr)_{CHUR} = 0.7045$ (DePaolo, 1988); $(^{147}Sm/^{144}Nd)_{CHUR} = 0.1967$ (Jacobsen and Wasserburg, 1980); $(^{143}Nd/^{144}Nd)_{CHUR} = 0.512638$ (Goldstein et al., 1984)] was used for the calculations. $\lambda_{Rb} = 1.42 \times 10^{-11}$ year^{-1} (Steiger and Jager, 1977); $\lambda_{Sm} = 6.54 \times 10^{-12}$ year^{-1} (Lugmair and Marti, 1978). Both εSr(i) and εNd(i) were obtained by using the average ages in the volcanic fields (Supplementary Data Table A.1).

as a consequence of the southward subduction of Asian continental lithosphere since 25 Ma (Fig. 2b), and northward flat slab subduction of Indian lithosphere from 55 Ma to 8 Ma (Fig. 2a), followed by steep subduction of the Indian slab since 8 Ma (Fig. 2c) (Li, 2008; Negredo et al., 2007; Zhao et al., 2010). The Asian mélange component does not appear to introduce radiogenic $^{87}Sr/^{86}Sr$ (Fig. 9) but does have low $^{143}Nd/^{144}Nd$, reflecting the isotopic composition of the trench sediments derived from the Asian continent. The incorporation of the Indian mélange component into the source of the potassic magmas may postdate the addition of the Asian mélange component, linked to the onset of steep subduction of the Indian slab since 8 Ma.

The mantle-normalized incompatible trace element pattern of average mélange rocks reported by Marschall and Schumacher (2012) is similar to those of the K-rich magmas in NW Tibet, characterized by enrichment in LILE and significant depletion in Nb, Ta and Ti (Fig. 7f). The compositions of mélange rocks (Marschall and Schumacher, 2012) are also consistent with those of the K-rich volcanic rocks in a Ce/Pb vs Nb/La diagram (Fig. 8d). These similarities support the role of mélange components in the petrogenesis of the K-rich magmas.

The second stage of the model involves the diapiric transportation of buoyant, low-density, enriched mélange domains into the shallow mantle, effectively underplating the base of the Tibetan lithosphere (Fig. 2). The absence of K-rich magmatism in NW Tibet during the period 25–8 Ma suggests that the mantle was too cool for melting of the underplated mélange at this stage (Fig. 2b). However, Asian mélange underplating could have caused uplift of the northwestern Tibetan Plateau during this period. We have no way of knowing when underplating of Indian mélange material beneath the Songpan-Ganzi terrane commenced; our suggestion in Fig. 2(c) is that it may have occurred slightly later. The onset of magma generation at ~8 Ma clearly requires a trigger to induce adiabatic upwelling in the sub-lithospheric mantle. We attribute this to the steep and deep subduction of the Indian slab beneath NW Tibet since 8 Ma.

The Sr–Nd–Pb isotope and trace element compositions of the potassic magmatic rocks indicate variable inputs from Asian and Indian mélange components from south to north. The Indian mélange component dominates in the southern subgroup magmas, whereas the Asian mélange component dominates in the northern subgroup (Figs. 2, 8 and 9). The central subgroup magmas exhibit mixed characteristics with evidence of derivation from a highly enriched mantle source; this may explain the long duration of magma generation and the presence of the active Ashi volcano (Fig. 2). It is not possible to quantify the proportions of the different mélange components which contribute to the source of the potassic magmas as the bulk composition, mineralogy and melting behavior of these components is unknown.

The synchronous (~8 Ma) onset of K-rich magmatism and the beginning of steep subduction of the Indian continental lithosphere beneath NW Tibet suggest that the near vertical subduction of the Indian slab

Table 4
Pb isotope compositions of the post-collisional potassium-rich magmatic rocks in NW Tibet.

Field no.	Sample no.	Field name	$^{206}Pb/^{204}Pb$	$^{207}Pb/^{204}Pb$	$^{208}Pb/^{204}Pb$	$^{238}U/^{204}Pb$	$^{235}U/^{204}Pb$	$^{232}Th/^{204}Pb$	$(^{206}Pb/^{204}Pb)_i$	$(^{207}Pb/^{204}Pb)_i$	$(^{208}Pb/^{204}Pb)_i$
1	CT09	Tianshuihai	18.742	15.727	39.184	9.182	0.067	42.970	18.735	15.727	39.173
1	CT12	Tianshuihai	18.736	15.684	39.132	11.527	0.085	149.442	18.727	15.684	39.094
1	CT17	Tianshuihai	18.704	15.713	39.145	7.167	0.053	42.469	18.698	15.713	39.134
1	CT05	Tianshuihai	18.727	15.673	39.227	12.000	0.088	56.839	18.717	15.673	39.212
1	CT23	Tianshuihai	18.886	15.691	39.216	13.810	0.101	70.761	18.875	15.690	39.198
2	QS12	Quanshuigou	19.069	15.746	39.314	9.228	0.068	97.078	19.062	15.746	39.289
2	QS27	Quanshuigou	18.714	15.696	39.115	10.779	0.079	99.694	18.705	15.696	39.089
2	QS19	Quanshuigou	18.942	15.674	38.986	11.025	0.081	228.407	18.933	15.674	38.927
2	QS23	Quanshuigou	18.881	15.658	39.037	12.546	0.092	167.281	18.871	15.658	38.994
2	QS18	Quanshuigou	18.812	15.715	39.276	7.101	0.052	99.328	18.806	15.715	39.250
2	QS24	Quanshuigou	18.894	15.643	39.028	5.737	0.042	135.395	18.889	15.643	38.993
3	KY03	Keliya	18.726	15.630	38.825	8.716	0.064	117.153	18.725	15.630	38.822
3	KY02	Keliya	18.751	15.641	39.057	14.259	0.105	124.959	18.750	15.641	39.054
3	KY06	Keliya	18.905	15.593	39.016	8.446	0.062	132.223	18.904	15.593	39.012
3	KY01	Keliya	18.877	15.634	38.945	18.032	0.132	164.405	18.875	15.634	38.940
4	HS041	Heishibei	18.942	15.867	39.461	15.494	0.114	56.512	18.938	15.867	39.456
4	HS046	Heishibei	18.975	15.948	39.583	10.381	0.076	41.324	18.972	15.948	39.579
4	HS047	Heishibei	19.012	15.827	39.126	7.633	0.056	54.099	19.010	15.827	39.121
4	HS028	Heishibei	19.014	15.746	38.830	9.340	0.069	112.063	19.011	15.746	38.820
5	AH607	Ashikule	18.783	15.685	38.951	6.257	0.046	25.760	18.782	15.685	38.950
5	AH605	Ashikule	18.818	15.664	38.975	5.467	0.040	25.278	18.817	15.664	38.974
5	AH609	Ashikule	18.705	15.673	38.904	8.962	0.066	36.425	18.704	15.673	38.902
5	AH602	Ashikule	18.766	15.649	38.983	6.989	0.051	27.692	18.765	15.649	38.982
5	AH618	Ashikule	18.837	15.682	39.064	8.005	0.059	31.600	18.836	15.682	39.062
5	AH615	Ashikule	18.714	15.627	38.810	5.210	0.038	21.631	18.713	15.627	38.809
7	YS74	Dahongliutan	18.713	15.657	38.702	10.066	0.074	45.046	18.707	15.657	38.693
7	YS78	Dahongliutan	18.752	15.683	38.947	12.391	0.091	52.389	18.745	15.683	38.937
7	YS05	Dahongliutan	18.781	15.672	38.823	13.457	0.099	26.359	18.773	15.672	38.818
7	YS79	Dahongliutan	18.764	15.705	38.947	10.852	0.080	40.427	18.758	15.705	38.939
7	YS07	Dahongliutan	18.776	15.731	39.215	13.731	0.101	61.422	18.768	15.731	39.203
8	KX44	Kangxiwa	18.819	15.654	38.995	7.266	0.053	30.405	18.815	15.654	38.990
8	KX51	Kangxiwa	18.776	15.631	38.863	12.454	0.091	22.359	18.770	15.631	38.859
8	KX80	Kangxiwa	18.804	15.585	38.672	7.413	0.054	24.241	18.800	15.585	38.668
8	KX49	Kangxiwa	18.807	15.679	38.846	9.302	0.068	29.608	18.802	15.679	38.841
8	KX62	Kangxiwa	18.812	15.647	38.809	9.112	0.067	23.449	18.807	15.647	38.805
9	PL53	Pulu	18.776	15.653	38.721	6.203	0.046	25.761	18.775	15.653	38.719
9	PL61	Pulu	18.752	15.691	38.657	6.982	0.051	20.326	18.751	15.691	38.656
9	PL3	Pulu	18.787	15.572	39.135	3.346	0.025	14.903	18.786	15.572	39.134
9	PL18	Pulu	18.751	15.675	38.978	4.041	0.030	27.842	18.750	15.675	38.976
9	PL92	Pulu	18.785	15.628	38.824	3.879	0.028	31.077	18.784	15.628	38.822
9	PL43	Pulu	18.815	15.637	38.946	3.630	0.027	17.322	18.814	15.637	38.945

Field no. refers to number of volcanic field in Fig. 1. $\lambda_{U238} = 0.155125 \times 10^{-9}$ year^{-1}, $\lambda_{U235} = 0.98485 \times 10^{-9}$ year^{-1} and $\lambda_{Th232} = 0.049475 \times 10^{-9}$ year^{-1} (Steiger and Jager, 1977). $(^{207}Pb/^{204}Pb)_{NHRL} = 0.1084 \times (^{206}Pb/^{204}Pb)_i + 13.491$ (Hart, 1984); $(^{208}Pb/^{204}Pb)_{NHRL} = 1.209 \times (^{206}Pb/^{204}Pb)_i + 15.627$ (Hart, 1984). Initial Pb isotope ratios were obtained by using the average ages of the volcanic fields (Supplementary Data Table A.1).

provided the critical trigger for melting of the underplated mélanges (Fig. 2c). Steep subduction of the Indian slab beneath NW Tibet has been attributed to a sharp change in the convergence angle between India and Asia since 8 Ma (Lee and Lawver, 1995).

6.4. Generic application of the model to other areas of the Alpine–Himalayan orogeny

Prelević et al (2013) have recently proposed a similar mélange model to explain the source of post-collisional potassic magmatism throughout the Alpine–Himalayan orogenic belt. The mélange is considered to contain a mixture of fore-arc depleted harzburgite and terrigenous trench sediments. They propose that such material becomes accreted beneath the lithosphere of the upper plate during continental collision.

Similar REE patterns to those of the potassic rocks of NW Tibet have been reported for potassic rocks within the Mediterranean area from SE Spain (Conticelli et al., 2009; Contini et al., 1993; Nixon et al., 1984; Prelević et al., 2008) and central Italy (Boari et al., 2009; Conticelli et al., 2009, 2010, 2013; Gasperini et al., 2002; Owen, 2008; Perini et al., 2004; Rogers et al., 1985). The potassic rocks from SE Spain (Conticelli et al., 2009; Prelević et al., 2008; Venturelli et al., 1984) and central Italy (Conticelli and Peccerillo, 1992; Conticelli et al., 2009, 2010, 2013; Gasperini et al., 2002) also have similar trace element patterns to the NW Tibetan magmas. Moreover, the Sr–Nd–Pb isotope compositions of the K-rich rocks in NW Tibet are similar to those of the potassic rocks from SE Spain (Conticelli et al., 2009; Nelson, 1992; Prelević et al., 2008, 2010, 2013) and central Italy (Boari et al., 2009; Conticelli et al., 2009, 2010, 2011, 2013; Gasperini et al., 2002; Owen, 2008; Perini et al., 2004; Prelević et al., 2010, 2013). These geochemical similarities strongly support a similar petrogenesis.

7. Conclusions

Based on the major and trace element and Sr–Nd–Pb isotopic compositions of post-collisional potassic magmatic rocks in NW Tibet, combined with geochronological data from the literature, we propose a two-stage model to explain their petrogenesis. The enriched source of the magmas is considered to comprise a mixture of subduction channel mélange material derived from opposing Indian and Asian subduction systems; this material became underplated beneath the continental lithosphere of the Songpan-Ganzi terrane of NW Tibet. The Indian and Asian mélanges carry the distinctive geochemical and isotopic signature of subducted terrigenous trench sediments, derived from the respective Indian and Asian continental basements, mixed with hydrated mantle material from the local mantle wedges. Partial melting of the underplated mélange may have been triggered by asthenospheric upwelling linked to the onset of steep subduction of the Indian slab at ~8 Ma.

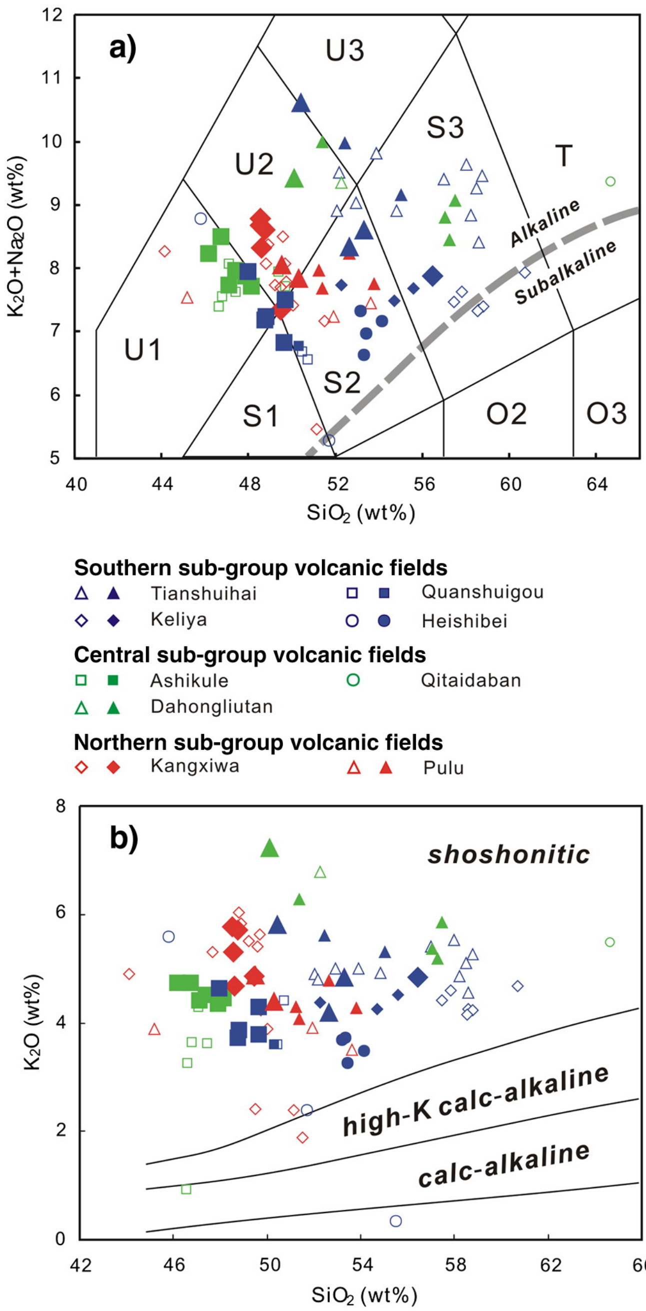

Fig. 5. (a) $K_2O + Na_2O$ (wt %) vs SiO_2 (wt %) variations in the K-rich igneous rocks of NW Tibet. All data plotted have been recalculated to 100 wt.% on a volatile-free basis (Supplementary Data Table A.2). Classification boundaries are from Le Bas et al. (1986) and Le Maitre et al. (1989). Filled and open symbols represent, respectively, data from this study and the published data of Arnaud et al. (1992), Turner et al. (1993, 1996), Deng (1998), Liu et al. (2003), Williams et al. (2004), Wang et al. (2005), Guo et al. (2006), Zhang et al. (2008), Li (2008), Wang and Zhang (2011) and Yang (2011). Rock types shown by letters are as follows. S2: basaltic trachyandesite; S3: trachyandesite; U1: tephrite; U2: phonotephrite; U3: tephriphonolite. Large filled symbols represent the compositions of the most primitive mafic volcanic rocks (i.e. MgO > 6 wt.%) highlighted in this study. (b) K_2O (wt %) vs SiO_2 (wt %) diagram for the same samples plotted in (a). The dividing lines show the classification boundaries from Rickwood (1989) and Le Maitre et al. (2002). Data sources and symbols are as in (a).

Acknowledgments

This study was supported by a grant from special project of Chinese Academy of Sciences (XDB03010600), grants from the National Natural Science Foundation of China (NSFC) (No: 41020124002 and 41130314) and by a joint project between the Royal Society of London and NSFC. We are grateful to Drs X. Chen and W. Guo for their help.

Appendix A. Supplementary data

Supplementary data to this article can be found online at http://dx.doi.org/10.1016/j.lithos.2014.03.020.

References

Ahmad, T., Harris, N., Bickle, M., Chapman, H., Bunbury, J., Prince, C., 2000. Isotopic constraints on the structural relationships between the Lesser Himalayan Series and the High Himalayan Crystalline Series, Garhwal Himalaya. Geological Society of America Bulletin 112, 467–477.

Arnaud, N.O., Vidal, P.H., Tapponnier, P., Matte, P.H., Deng, W.M., 1992. The high K_2O volcanism of northwestern Tibet: geochemistry and tectonic implications. Earth and Planetary Science Letters 111, 351–367.

Boari, E., Avanzinelli, R., Melluso, L., Giordano, G., Mattei, M., De Benedetti, A.A., Morra, V., Conticelli, S., 2009. Isotope geochemistry (Sr–Nd–Pb) and petrogenesis of leucite-bearing volcanic rocks from "ColliAlbani" volcano, Roman Magmatic Province, Central Italy: inferences on volcano evolution and magma genesis. Bulletin of Volcanology 71, 977–1005.

Brunsmann, A., Franz, G., Erzinger, J., Landwehr, D., 2000. Zoisite- and clinozoisite-segregations in metabasites (Tauern Window, Austria) as evidence for high-pressure fluid–rock interaction. Journal of Metamorphic Geology 18, 1–21.

Burtman, V.S., Molnar, P.H., 1993. Geological and geophysical evidence for deep subduction of continental crust beneath the Pamir. Geological Society of America Special Papers 281, 1–76.

Chen, J.L., Xu, J.F., Wang, B.D., Kang, Z.Q., Li, J., 2010. Origin of Cenozoic alkaline potassic volcanic rocks at KonglongXiang, Lhasa terrane, Tibetan Plateau: products of partial melting of a mafic lower-crustal source? Chemical Geology 273, 286–299.

Chung, S.L., Chu, M.F., Zhang, Y., Xie, Y., Lo, C.H., Lee, T.Y., Lan, C.Y., Li, X., Zhang, Q., Wang, Y., 2005. Tibetan tectonic evolution inferred from spatial and temporal variations in post-collisional magmatism. Earth-Science Reviews 68, 173–196.

Class, C., Miller, D.M., Goldstein, S.L., Langmuir, C.H., 2000. Distinguishing melt and fluid subduction components in Umnak Volcanics, Aleutian Arc. Geochemistry, Geophysics, Geosystems 1, 1004. http://dx.doi.org/10.1029/1999GC000010.

Conticelli, S., Peccerillo, A., 1992. Petrology and geochemistry of potassic and ultrapotassic volcanism in central Italy: petrogenesis and inferences on the evolution of the mantle sources. Lithos 28, 221–240.

Conticelli, S., Guarnieri, L., Farinelli, A., Mattei, M., Avanzinelli, R., Bianchini, G., Boari, E., Tommasini, S., Tiepolo, M., Prelević, D., Venturelli, G., 2009. Trace elements and Sr–Nd–Pb isotopes of K-rich, shoshonitic, and calc-alkaline magmatism of the Western Mediterranean Region: genesis of ultrapotassic to calc-alkaline magmatic associations in a post-collisional geodynamic setting. Lithos 107, 68–92.

Conticelli, S., Laurenzi, M., Giordano, G., Mattei, M., Avanzinelli, R., Melluso, L., Tommasini, S., Boari, E., Cifelli, F., Perini, G., 2010. Leucite-bearing (kamafugitic/leucititic) and-free (lamproitic) ultrapotassic rocks and associated shoshonites from Italy: constraints on petrogenesis and geodynamics. In: Beltrando, M., Peccerillo, A., Mattei, M., Conticelli, S., Doglioni, C. (Eds.), The Geology of Italy: Tectonics and Life Along Plate MarginsJournal of the Virtual Explorer 36. http://dx.doi.org/10.3809/jvirtex.2010.00251 (paper 20).

Conticelli, S., Avanzinelli, R., Marchionni, S., Tommasini, S., Melluso, L., 2011. Sr–Nd–Pb isotopes from the Radicofani Volcano, Central Italy: constraints on heterogeneities in a veined mantle responsible for the shift from ultrapotassicshoshonite to basaltic andesite magmas in a post-collisional setting. Mineralogy and Petrology 103, 123–148.

Conticelli, S., Avanzinelli, R., Poli, G., Braschi, E., Giordano, G., 2013. Shift from lamproite-like to leucititic rocks: Sr–Nd–Pb isotope data from the Monte Cimino volcanic complex vs. the Vicostratovolcano, Central Italy. Chemical Geology 353, 246–266.

Contini, S., Venturelli, G., Toscani, L., Capedri, S., Barbieri, M., 1993. Cr–Zr–armalcolite-bearing lamproites of Cancarix, SE Spain. Mineralogical Magazine 57, 203–216.

Cooper, K.M., Reid, M.R., Dunbar, N., McIntosh, W., 2002. Origin of mafic magmas beneath Northwestern Tibet: constraints from ^{230}Th–^{238}U disequilibria. Geochemistry, Geophysics, Geosystems 3, 1–23.

Deng, W.M., 1998. Cenozoic Intraplate Volcanic Rocks in the Northern Qinghai-Xizang Plateau. Geological Publishing House, Beijing p. 180 (in Chinese with English abstract).

DePaolo, D.J., 1988. Neodymium Isotope Geochemistry: an Introduction. Springer, New York p. 230.

Ding, L., Kapp, P., Zhong, D., Deng, W., 2003. Cenozoic volcanism in Tibet: evidence for a transition from oceanic to continental subduction. Journal of Petrology 44, 1833–1865.

Ding, L., Kapp, P., Yue, Y., Lai, Q., 2007. Postcollisional calc-alkaline lavas and xenoliths from the southern Qiangtang terrane, central Tibet. Earth and Planetary Science Letters 254, 28–38.

Dupont-Nivet, G., Krijgsman, W., Langereis, C.G., Abels, H.A., Dai, S., Fang, X.M., 2007. Tibetan plateau aridification linked to global cooling at the Eocene–Oligocene transition. Nature 445, 635–638.

Elburg, M.A., Bergen, M.A., Hoogewerff, J., Foden, J., Vroon, P., Zulkarnain, I., Nasution, A., 2002. Geochemical trends across an arc–continent collision zone: magma sources and slab-wedge transfer processes below the Pantar Strait volcanoes, Indonesia. Geochimica et Cosmochimica Acta 66, 2771–2789.

Feineman, M.D., Ryerson, F.J., DePaolo, D.J., Plank, T., 2007. Zoisite-aqueous fluid trace element partitioning with implications for subduction zone fluid composition. Chemical Geology 239, 250–265.

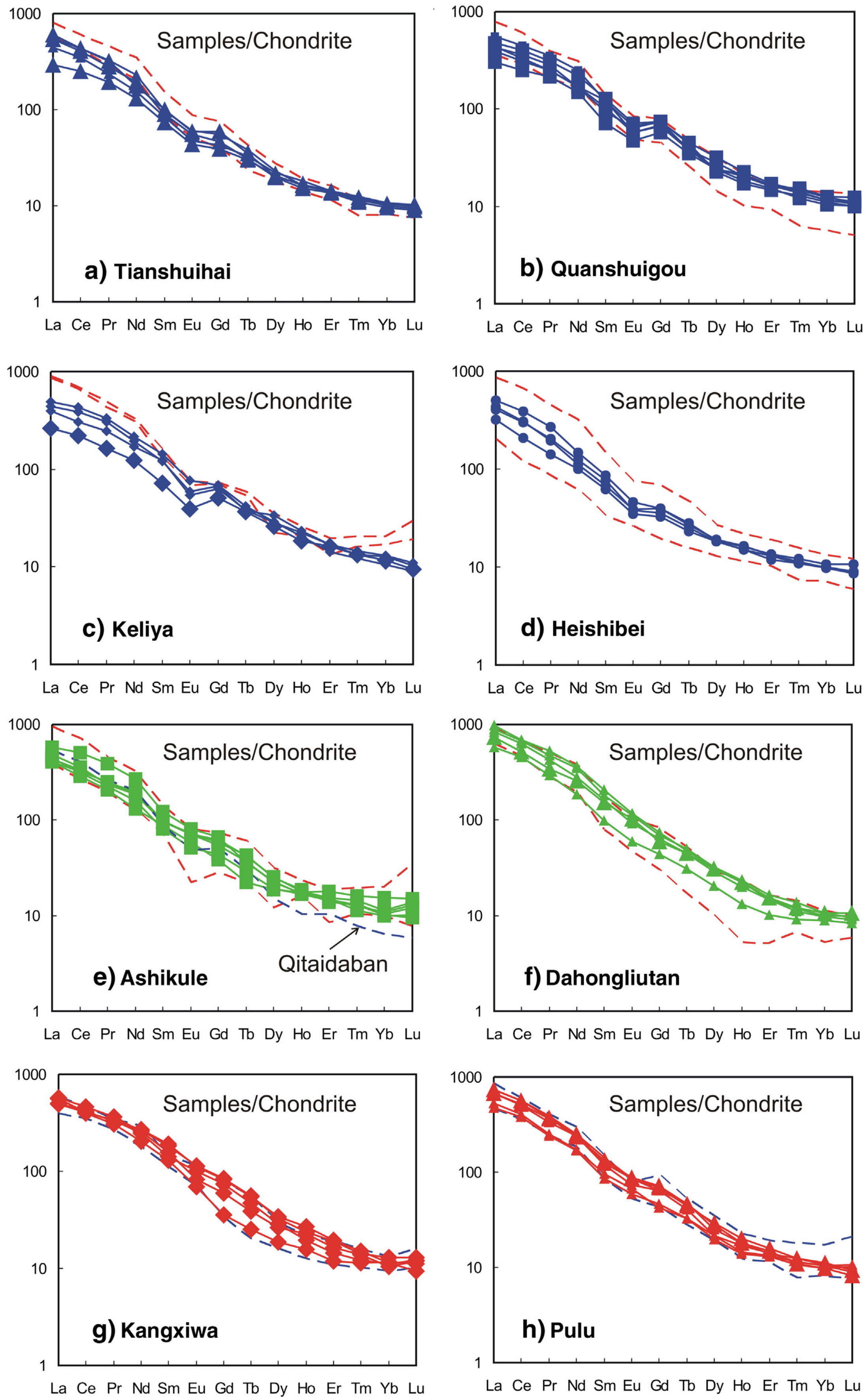

Fig. 6. Chondrite-normalized rare earth element patterns; normalization factors are from Sun and McDonough (1989). The dashed lines denote the range of previously published data for the post-collisional K-rich magmatic rocks in NW Tibet (Arnaud et al., 1992; Deng, 1998; Guo et al., 2006; Li, 2008; Liu et al., 2003; Turner et al., 1993, 1996; Wang and Zhang, 2011; Wang et al., 2005; Williams et al., 2004; Yang, 2011; Zhang et al., 2008). Data sources are as in Fig. 5(a).

Frei, D., Liebscher, A., Franz, G., Dulski, P., 2004. Trace element geochemistry of epidote minerals. Reviews in Mineralogy and Geochemistry 56, 553–605.
Garzione, C.N., 2008. Surface uplift of Tibet and Cenozoic global cooling. Geology 36, 1003–1004.
Gasperini, D., Blichert-Toft, J., Bosch, D., Del Moro, A., Macera, P., Albarède, F., 2002. Upwelling of deep mantle material through a plate window: evidence from the geochemistry of Italian basaltic volcanics. Journal of Geophysical Research 107, 2367. http://dx.doi.org/10.1029/2001jb000418.
Gerya, T.V., Stöckhert, B., Perchuk, A.L., 2002. Exhumation of high-pressure metamorphic rocks in a subduction channel: a numerical simulation. Tectonics 21, 1056. http://dx.doi.org/10.1029/2002TC001406.
Gill, J.B., 1981. Orogenic Andesites and Plate Tectonics. Springer, Berlin p. 390.
Goldstein, S.L., O'Nions, R.K., Hamilton, P.J., 1984. A Sm–Nd isotopic study of atmospheric dusts and particulates from major river systems. Earth and Planetary Science Letters 70, 221–236.
Govindaraju, K., 1994. Compilation of working values and sample description for 383 geostandards. Geostand Newsletter 18, 1–158.
Guillot, S., Hattori, K., Agard, P., Schwartz, S., Vidal, O., 2009. Exhumation processes in oceanic and continental subduction contexts: a review. In: Lallemand, S., Funiciello, F. (Eds.), Subduction Zone Geodynamics. Frontiers in Earth Sciences, pp. 175–205.
Guo, Z., Wilson, M., 2012. The Himalayan leucogranites: constraints on the nature of their crustal source region and geodynamic setting. Gondwana Research 22, 360–376.
Guo, Z., Hertogen, J., Liu, J., Pasteels, P., Boven, A., Punzalan, L., He, H., Luo, X., Zhang, W., 2005a. Potassic magmatism in western Sichuan and Yunnan provinces, SE Tibet,

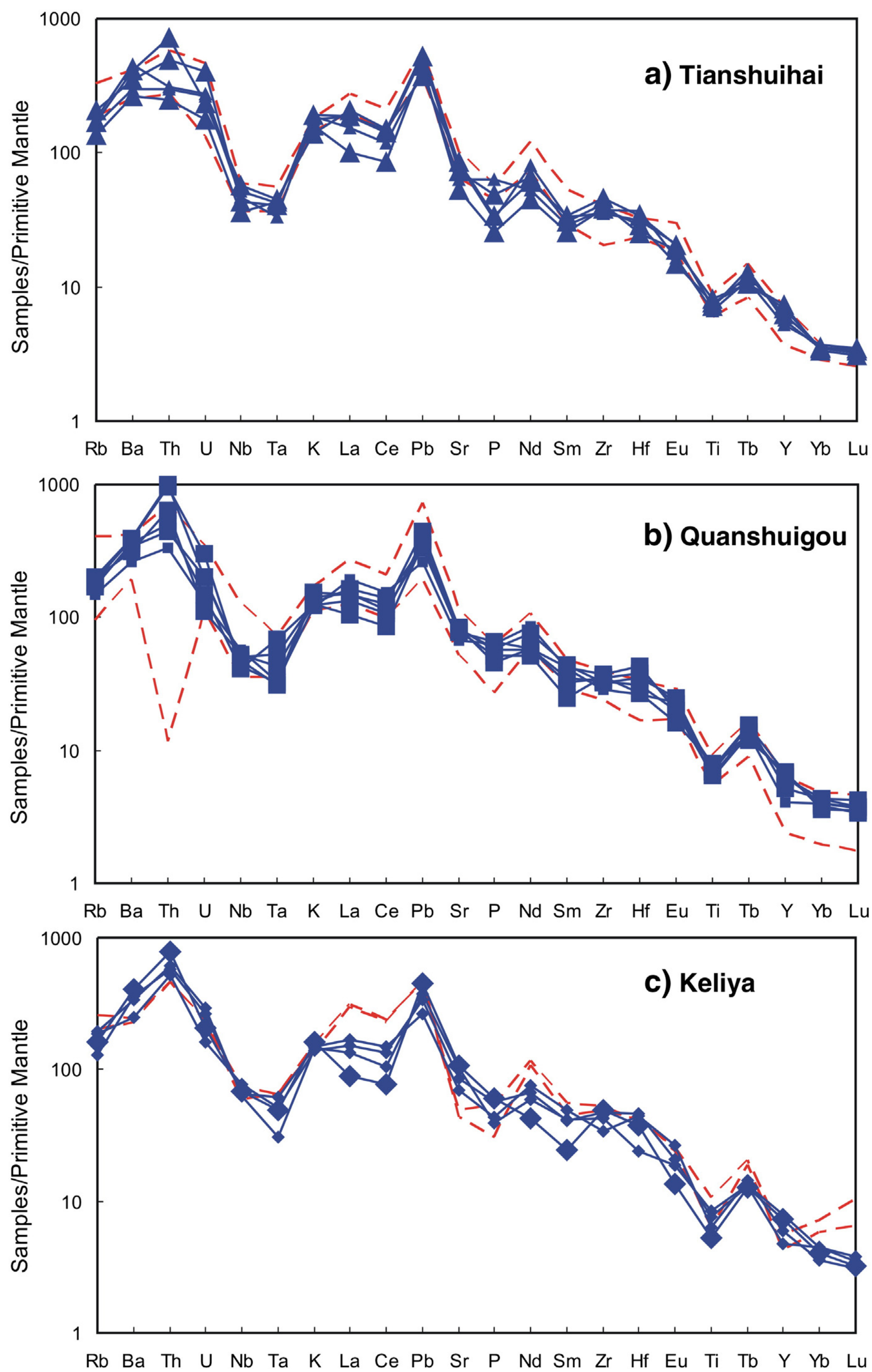

Fig. 7. Primitive mantle-normalized trace element patterns; normalization factors are from Sun and McDonough (1989). The dashed lines denote the range of previously published data for the post-collisional K-rich magmatic rocks in NW Tibet (Arnaud et al., 1992; Deng, 1998; Guo et al., 2006; Li, 2008; Liu et al., 2003; Turner et al., 1993, 1996; Wang and Zhang, 2011; Wang et al., 2005; Williams et al., 2004; Yang, 2011; Zhang et al., 2008). Data for the average composition of subduction channel mélange rocks in panel (f) are from Marschall and Schumacher (2012). Data sources are as in Fig. 5(a).

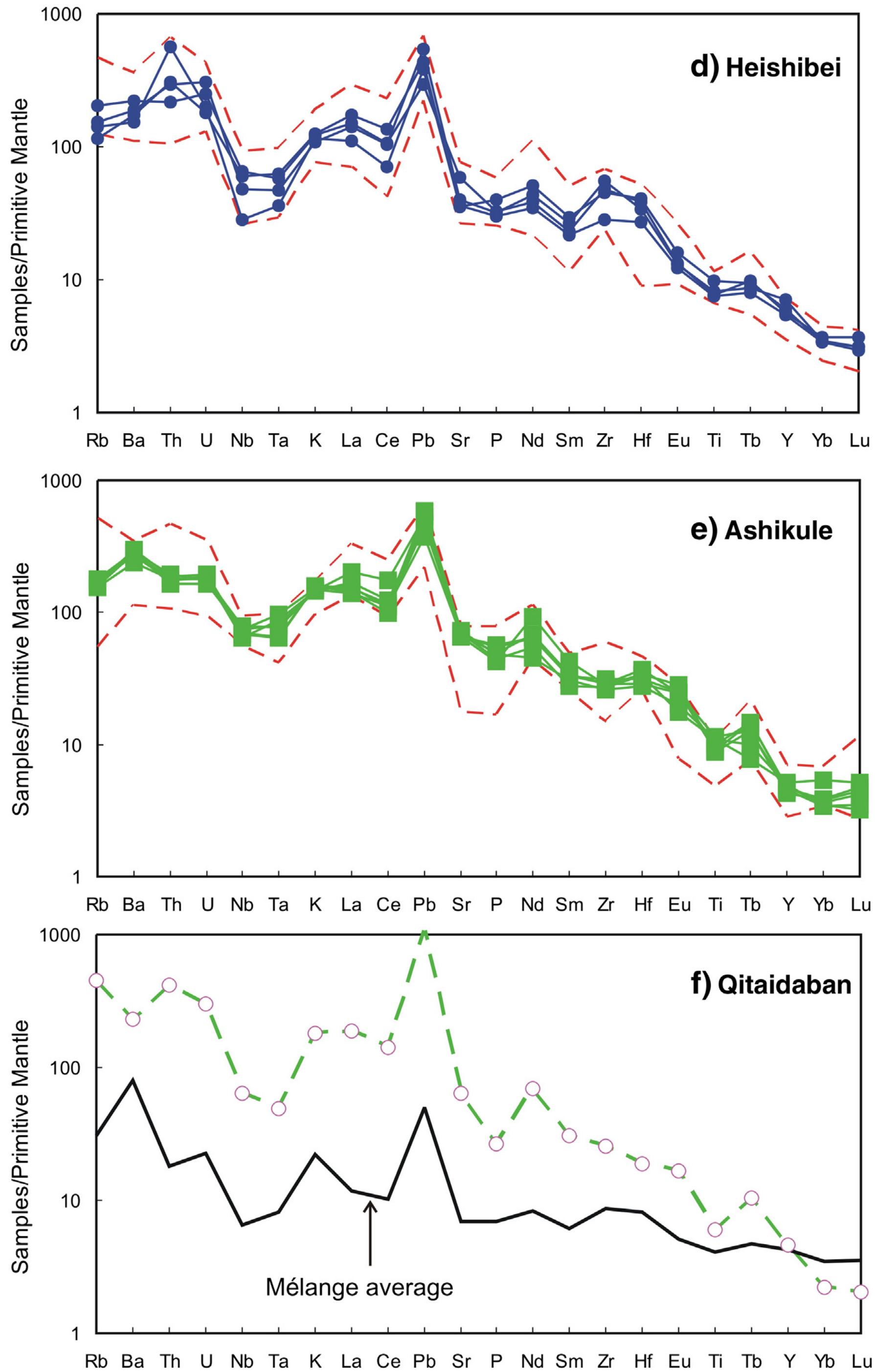

Fig. 7 (*continued*).

China: petrological and geochemical constraints on petrogenesis. Journal of Petrology 46, 33–78.

Guo, Z.J., Yin, A., Robinson, A., Jia, C.Z., 2005b. Geochronology and geochemistry of deep-drill-core samples from the basement of the central Tarim basin. Journal of Asian Earth Sciences 25, 45–56.

Guo, Z., Wilson, M., Liu, J., Mao, Q., 2006. Post-collisional, potassic and ultrapotassic magmatism of the northern Tibetan plateau: constraints on characteristics of the mantle source, geodynamic setting and uplift mechanisms. Journal of Petrology 47, 1177–1220.

Guo, Z., Wilson, M., Zhang, M., Cheng, Z., Zhang, L., 2013. Post-collisional, K-rich mafic magmatism in south Tibet: constraints on Indian slab-to-wedge transport processes and plateau uplift. Contributions to Mineralogy and Petrology 165, 1311–1340.

Hart, S.R., 1984. A large-scale isotope anomaly in the Southern Hemisphere mantle. Nature 309, 753–757.

Hawkesworth, C.J., Turner, S.P., McDermott, F., Peate, D.W., van Calsteren, P., 1997. U–Th isotopes in arc magmas: implications for element transfer from the subducted crust. Science 276, 551–555.

Hickmott, D.D., Sorensen, S.S., Rogers, P.S.Z., 1992. Metasomatism in a subduction complex: constraints from microanalysis of trace elements in minerals from garnet amphibolite from the Catalina Schist. Geology 20, 347–350.

Inger, S., Harris, N., 1993. Geochemical constraints on leucogranite magmatism in the Langtang valley, Nepal Himalaya. Journal of Petrology 34, 345–368.

Jacobsen, S.B., Wasserburg, G.J., 1980. Sm–Nd isotopic evolution of chondrites. Earth and Planetary Science Letters 50, 139–155.

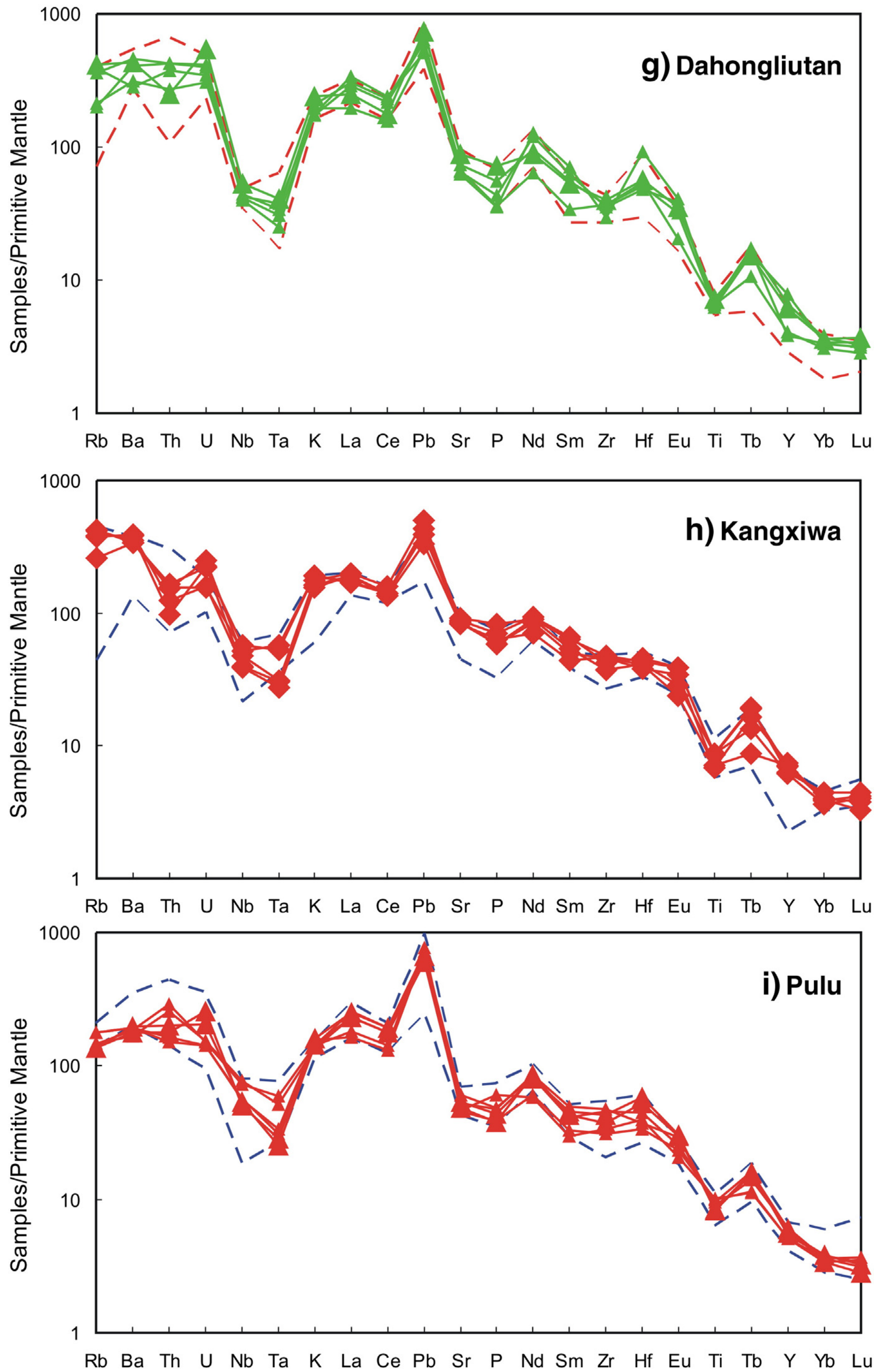

Fig. 7 (*continued*).

Jiang, C.Y., Jia, C.Z., Li, L.C., Zhang, P.B., Lu, D.R., Bai, K.Y., 2004. Source of the Fe-riched-type high-Mg magma in Mazhartag region, Xinjiang. Acta Geologica Sinica 78, 770–780 (in Chinese with English abstract).

Johnson, M.C., Plank, T., 1999. Dehydration and melting experiments constrain the fate of subducted sediments. Geochemistry, Geophysics, Geosystems 1, 1007. http://dx.doi.org/10.1029/1999GC000014.

Le Bas, M.J., Le Maitre, R.W., Streckeisen, A., Zanettin, B., 1986. A chemical classification of volcanic rocks based on the total alkali–silica diagram. Journal of Petrology 27, 745–750.

Le Maitre, R.W., Bateman, P., Dudek, A., Keller, J., Lameyre, J., Le Bas, M.J., Sabine, P.A., Schmid, R., Sorensen, H., Streckeisen, A., Woolley, A.R., Zanettin, B., 1989. A Classification of Igneous Rocks and a Glossary of Terms. Blackwell Scientific, Oxford p. 236.

Le Maitre, R.W., Streckeisen, A., Zanettin, B., Le Bas, M.J., Bonin, B., Bateman, P., Bellieni, G., Dudek, A., Efremova, S.A., Keller, J., Lameyre, J., Sabine, P.A., Schmid, R., Søensen, H., Woolley, A.R., 2002. Igneous Rocks: a Classification Glossary of Terms. Cambridge University Press, Cambridge p. 236.

Lee, T.Y., Lawver, L.A., 1995. Cenozoic plate reconstruction of southeast Asia. Tectonophysics 251, 85–138.

Li, D.P., 2008. Tectonic Deformation on the Northwestern Margin of Tibetan Plateau During Pliocene–Pleistocene and Uplift of the Tibetan Plateau. Institute of Geology Chinese Academy of the Geological Science, Beijing, China (Unpublished PhD Thesis, 211 pp.) (in Chinese with English abstract).

Liu, J., 1999. Volcanoes in China. Science Press, Beijing p. 219 (in Chinese).

Liu, S., Hu, R.Z., Chi, X.G., Li, C., Feng, C.X., 2003. Geochemistry, series subdivision and petrogenetic interpretation of Cenozoic volcanic rocks in Northern Tibet. Geological Journal of China University 9, 279–292 (in Chinese with English abstract).

Lugmair, G.W., Marti, K., 1978. Lunar initial $^{143}Nd/^{144}Nd$: differential evolution of the lunar crust and mantle. Earth and Planetary Science Letters 39, 349–357.

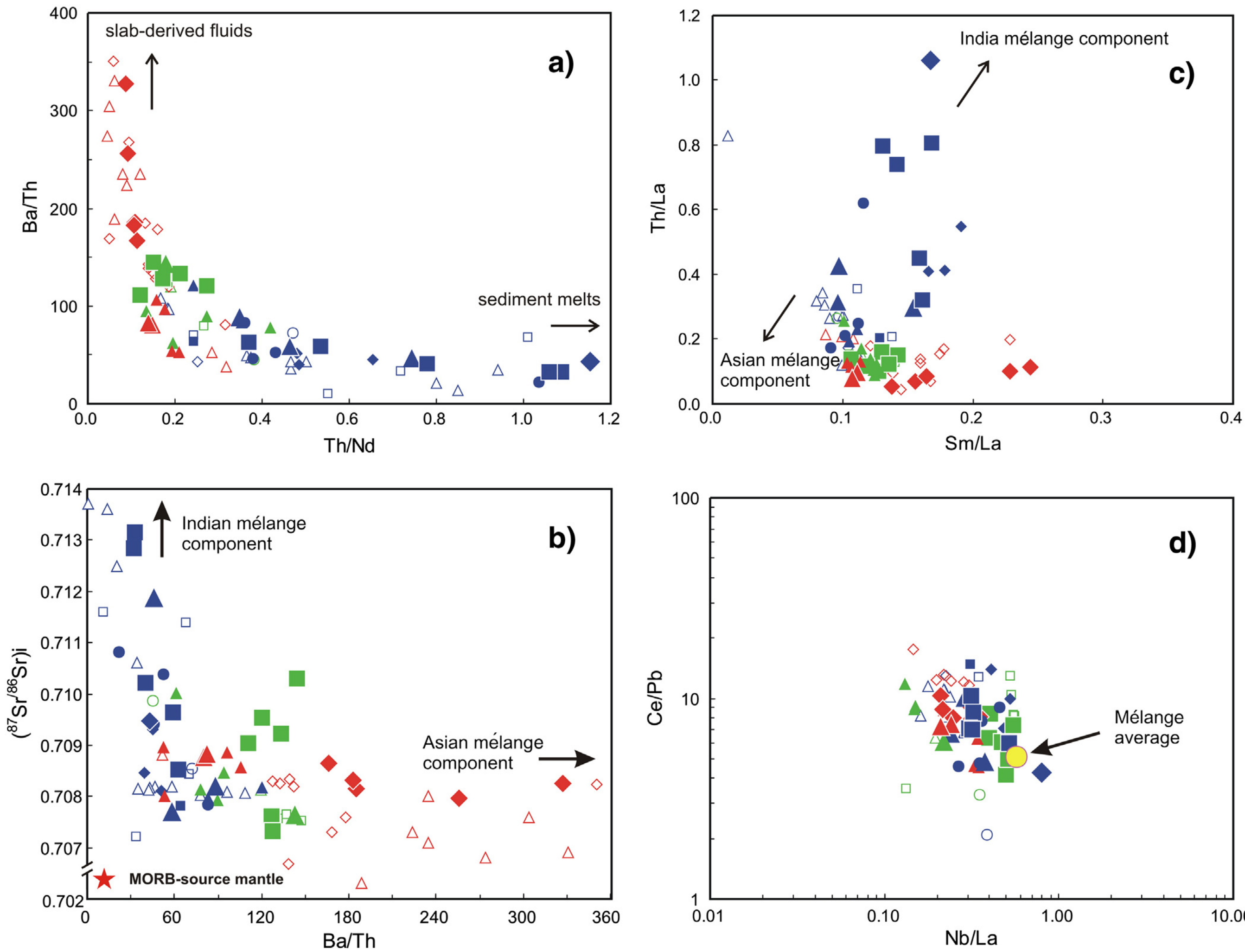

Fig. 8. (a) Ba/Th vs Th/Nd. (b) ($^{87}Sr/^{86}Sr$)$_i$ vs Ba/Th. (c) Th/La vs Sm/La. (d) Ce/Pb vs Nb/La. All data plotted as filled symbols are from Supplementary Data Table A.2 and Table 3. The red star represents the composition of MORB-source mantle (Sun and McDonough, 1989) in (b). The red circle filled with yellow represents the average composition of mélange rocks (Marschall and Schumacher, 2012) in (d). Symbols are as in Fig. 5(a). (For interpretation of the references to color in this figure legend, the reader is referred to the web version of this article.)

Marschall, H.R., Schumacher, J.C., 2012. Arc magmas sourced from mélange diapirs in subduction zones. Nature Geoscience 5, 862–867.
McCulloch, M.T., Black, L.P., 1984. Sm–Nd isotope systematics of Enderby Land granulites and evidence for the redistribution of Sm and Nd during metamorphism. Earth and Planetary Science Letters 71, 46–58.
Mo, X., Zhao, Z., Deng, J., Flower, M., Yu, X., Luo, Z., Li, Y., Zhou, S., Dong, G., Zhu, D., 2006. Petrology and geochemistry of postcollisional volcanic rocks from the Tibetan plateau: implications for lithosphere heterogeneity and collision-induced asthenospheric mantle flow. In: Dilek, Y., Pavlides, S. (Eds.), Postcollisional tectonics and Magmatism in the Mediterranean Region and Asia. Geological Society of America Special Papers, 409, pp. 507–530.
Negredo, A.M., Replumaz, A., Villaseñor, A., Guillot, S., 2007. Modeling the evolution of continental subduction processes in the Pamir–Hindu Kush region. Earth and Planetary Science Letters 259, 212–225.
Nelson, D.R., 1992. Isotopic characteristics of potassic rocks: evidence for the involvement of subducted sediments in magma genesis. Lithos 28, 403–420.
Nixon, P., Thirlwall, M., Buckley, F., Davies, C., 1984. Spanish and Western Australian lamproites: aspects of whole rock geochemistry. In: Kornprobst, J. (Ed.), Proceedings of the Third International Kimberlite Conference: I. Kimberlites and Related Rocks. Elsevier, Amsterdam, pp. 285–296.
Owen, J.P., 2008. Geochemistry of lamprophyres from the Western Alps, Italy: implications for the origin of an enriched isotopic component in the Italian mantle. Contributions to Mineralogy and Petrology 155, 341–362.
Pan, G., Ding, J., Yao, D., Wang, L., 2004. An Introduction of Geological Map of the Tibetan Plateau and Neighbouring Area. Chengdu Map Press, Chengdu, China p. 133 (in Chinese).
Pearce, J.A., 1983. Role of the sub-continental lithosphere in magma genesis at active continental margins. In: Hawkesworth, C.J., Norry, M.J. (Eds.), Continental Basalts and Mantle Xenoliths. Shiva Geology Series, pp. 230–249.
Pearce, J.A., Mei, H., 1988. Volcanic rocks of the 1985 Tibet geotraverse: Lhasa to Golmud. Philosophical Transactions of the Royal Society of London A327, 169–201.
Pearce, J.A., Parkinson, I.J., 1993. Trace element models for mantle melting: application to volcanic arc petrogenesis. In: Prichard, H.M., Alabaster, T., Harris, N.B.W., Neary, C.R. (Eds.), Magmatic Processes and Plate Tectonics. Geological Society of London, Special Publications, 76, pp. 373–403.
Perini, G., Francalanci, L., Davidson, J.P., Conticelli, S., 2004. Evolution and genesis of magmas from Vico Volcano, Central Italy: multiple differentiation pathways and variable parental magmas. Journal of Petrology 45, 139–182.
Prelević, D., Foley, S.F., Romer, R., Conticelli, S., 2008. Mediterranean Tertiary lamproites derived from multiple source components in postcollisional geodynamics. Geochimica et Cosmochimica Acta 72, 2125–2156.
Prelević, D., Akal, C., Romer, R.L., Foley, S.F., 2010. Lamproites as indicators of accretion and/or shallow subduction in the assembly of south-western Anatolia, Turkey. Terra Nova 22, 443–452.
Prelević, D., Jacob, D.E., Foley, S.F., 2013. Recycling plus: a new recipe for the formation of Alpine–Himalayan orogenic mantle lithosphere. Earth and Planetary Science Letters 362, 187–197.
Raymo, M., Ruddiman, W.F., 1992. Tectonic forcing of late Cenozoic climate. Nature 359, 117–122.
Richards, A., Argles, T., Harris, N., Parrish, R., Ahmad, T., Darbyshire, F., Draganits, E., 2005. Himalayan architecture constrained by isotopic tracers from clastic sediments. Earth and Planetary Science Letters 236, 773–796.
Rickwood, P.C., 1989. Boundary lines within petrologic diagrams which use oxides of major and minor elements. Lithos 22, 247–263.
Roger, F., Tapponnier, P., Arnaud, N., Schärer, U., Brunel, M., Xu, Z.Q., Yang, J.S., 2000. An Eocene magmatic belt across central Tibet: mantle subduction triggered by the Indian collision? Terra Nova 12, 102–108.
Rogers, N.W., Hawkesworth, C.J., Parker, R.J., Marsh, J.S., 1985. The geochemistry of potassic lavas from Vulsini, central Italy and implications for mantle enrichment processes beneath the Roman region. Contributions to Mineralogy and Petrology 90, 244–257.
Searle, M.P., Elliott, J.R., Phillips, R.J., Chung, S.L., 2011. Crustal-lithospheric structure and continental extrusion of Tibet. Journal of the Geological Society 168, 633–672.

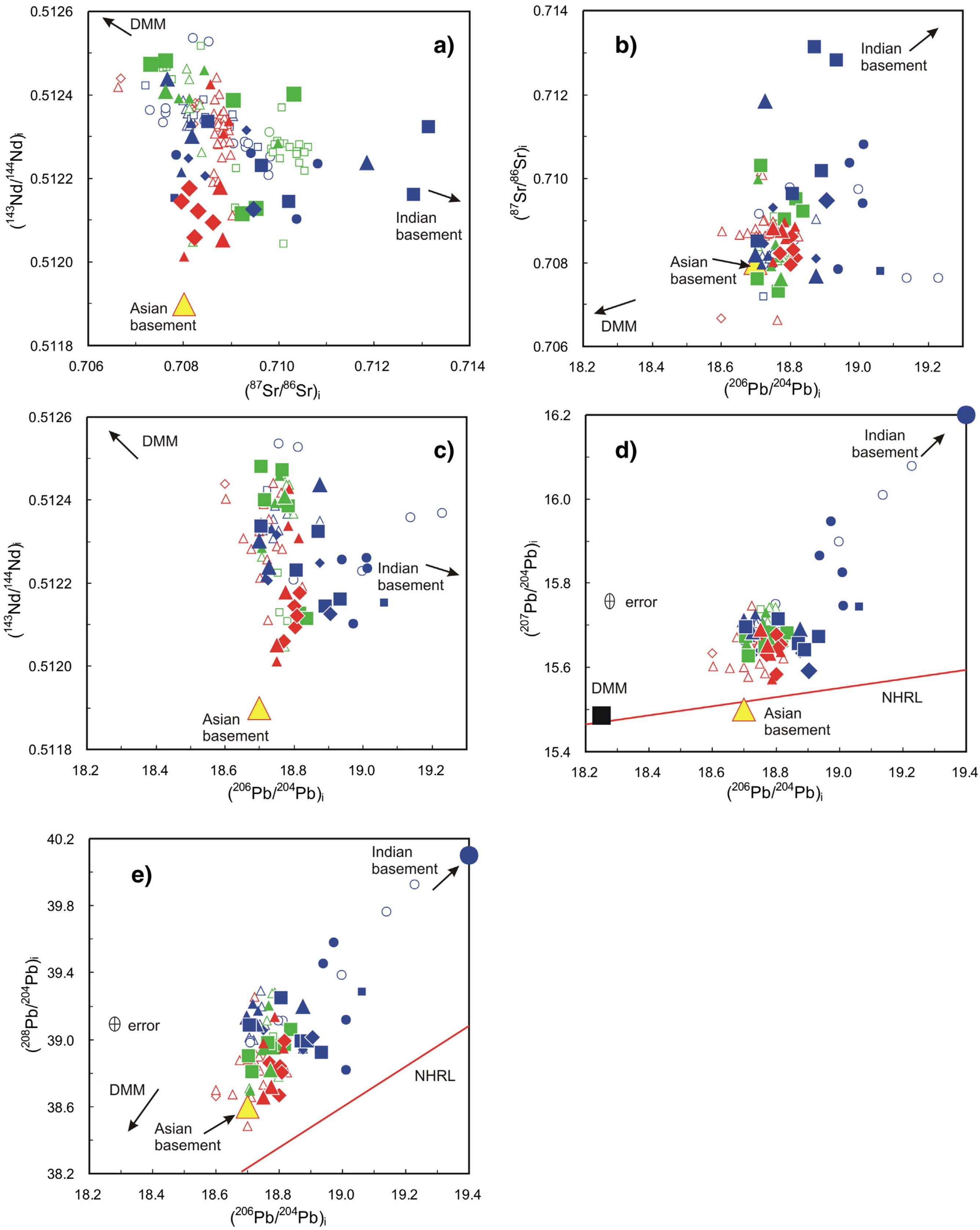

Fig. 9. (a) $(^{143}Nd/^{144}Nd)_i$ vs $(^{87}Sr/^{86}Sr)_i$. (b) $(^{87}Sr/^{86}Sr)_i$ vs $(^{206}Pb/^{204}Pb)_i$. (c) $(^{143}Nd/^{144}Nd)_i$ vs $(^{206}Pb/^{204}Pb)_i$. (d) $(^{207}Pb/^{204}Pb)_i$ vs $(^{206}Pb/^{204}Pb)_i$. (e) $(^{208}Pb/^{204}Pb)_i$ vs $(^{206}Pb/^{204}Pb)_i$. The Sr–Nd–Pb isotope data for samples from this study are from Tables 3 and Table 4. Symbols are as in Fig. 5(a). Arrows point towards the composition of depleted MORB-source mantle (DMM) (Workman and Hart, 2005), Indian continental basement (Ahmad et al., 2000; Guo and Wilson, 2012; Inger and Harris, 1993; Richards et al., 2005) and Asian basement (Guo et al., 2005b; Jiang et al., 2004; Zhang et al., 2004; Zhang et al., 2009). The large black square, large blue circle, and large yellow-filled red triangle represent the compositions of depleted MORB-source mantle (DMM), Indian basement and Asian basement, respectively. The NHRL (Northern Hemisphere Reference Line) is shown for reference in (d) and (e) (Hart, 1984). (For interpretation of the references to color in this figure legend, the reader is referred to the web version of this article.)

Spandler, C., Hermann, J., Arculus, R., Mavrogenes, J., 2003. Redistribution of trace elements during prograde metamorphism from lawsonite blueschist to eclogite facies; implications for deep subduction-zone processes. Contributions to Mineralogy and Petrology 146, 205–222.
Steiger, R.H., Jager, E., 1977. Subcommission on geochronology: convention of the use of decay constants in geo- and cosmochronology. Earth and Planetary Science Letters 36, 259–362.
Sun, S.-S., McDonough, W.F., 1989. Chemical and isotopic systematics of ocean basalts: implications for mantle composition and processes. In: Saunders, A.D., Norry, M.J. (Eds.), Magmatism in the Ocean Basins. Geological Society of London, Special Publications, 42, pp. 313–345.
Tatsumi, Y., Hamilton, D.L., Nesbitt, R.W., 1986. Chemical characteristics of fluid phase released from a subducted lithosphere and origin of arc magmas: evidence from high-pressure experiments and natural rocks. Journal of Volcanology and Geothermal Research 29, 293–309.
Tommasini, S., Avanzinelli, R., Conticelli, S., 2011. The Th/La and Sm/La conundrum of the Tethyan realm lamproites. Earth and Planetary Science Letters 301, 469–478.
Turner, S., Hawkesworth, C., Liu, J., Rogers, N., Kelley, S., van Calsteren, P., 1993. Timing of Tibetan uplift constrained by analysis of volcanic rocks. Nature 364, 50–54.
Turner, S., Arnaud, N., Liu, J., Rogers, N., Hawkesworth, C., Harris, N., Kelley, S., van Calsteren, P., Deng, W., 1996. Post-collision, shoshonitic volcanism on the Tibetan Plateau: implications for convective thinning of the lithosphere and the source of ocean island basalts. Journal of Petrology 37, 45–71.
Usui, T., Nakamura, E., Helmstaedt, H., 2006. Petrology and geochemistry of eclogite xenoliths from the Colorado Plateau: implications for the evolution of subducted oceanic crust. Journal of Petrology 47, 929–964.
Venturelli, G., Capedri, S., Di Battistini, G., Crawford, A., Kogarko, L.N., Celestini, S., 1984. The ultrapotassic rocks from southeastern Spain. Lithos 17, 37–54.
Wang, H.Y., Zhang, C.L., 2011. Age and geochemical characteristic of Quaternary volcanic rocks in the northwestern margin of Tibetan Plateau and their significance. Geological Bulletin of China 30, 1171–1181 (in Chinese with English abstract).
Wang, Q., Yang, W.B., Zhang, Z.F., Yang, Y.S., Wu, J.G., Dong, A.G., 2005. Geological characteristics of Neogene volcanic rocks in the Heishi North Lake area, northwestern Tibet and their implication for the Neogene tectonic evolution. Geological Bulletin of China 24, 80–86 (in Chinese with English abstract).
Wang, Q., Wyman, D.A., Xu, J., Dong, Y., Vasconcelos, P.M., Pearson, N., Wan, Y., Dong, H., Li, C., Yu, Y., Zhu, T., Feng, X., Zhang, Q., Zi, F., Chu, Z., 2008. Eocene melting of subducting continental crust and early uplifting of central Tibet: evidence from central-western Qiangtang high-K calc-alkaline andesites, dacites and rhyolites. Earth and Planetary Science Letters 272, 158–171.
Wang, Q., Wyman, D.A., Li, Z.X., Sun, W.D., Chung, S.L., Vasconcelos, P.M., Zhang, Q.Y., Dong, H., Yu, Y.S., Pearson, N., Qiu, H.N., Zhu, T.X., Feng, X.T., 2010. Eocene north–south trending dikes in central Tibet: new constraints on the timing of east–west extension with implications for early plateau uplift? Earth and Planetary Science Letters 298, 205–216.
Wang, Q., Chung, S.L., Li, X.H., Wyman, D., Li, Z.X., Sun, W.D., Qiu, H.N., Liu, Y.S., Zhu, Y.T., 2012. Crustal Melting and Flow beneath Northern Tibet: evidence from Mid-Miocene to Quaternary strongly peraluminous rhyolites in the Southern Kunlun Range. Journal of Petrology 58, 2523–2566.
Williams, H., Turner, S., Kelley, S., Harris, N., 2001. Age and composition of dikes in southern Tibet: new constraints on the timing of east–west extension and its relationship to postcollisional volcanism. Geology 29, 339–342.
Williams, H.M., Turner, S.P., Pearce, J.A., Kelley, S.P., Harris, N.B.W., 2004. Nature of the source regions for post-collisional, potassic magmatism in southern and northern Tibet from geochemical variations and inverse trace element modeling. Journal of Petrology 45, 555–607.
Woodhead, J.D., Hergt, J.M., Davidson, J.P., Eggins, S.M., 2001. Hafnium isotope evidence for 'conservative' element mobility during subduction zone processes. Earth and Planetary Science Letters 192, 331–346.
Workman, R.K., Hart, S.R., 2005. Major and trace element composition of the depleted MORB mantle (DMM). Earth and Planetary Science Letters 231, 53–72.
Yang, D., 2011. The $^{40}Ar/^{39}Ar$ Geochronology and Geochemistry Research on Cenozoic Volcanic Rocks of Hoh Xil and Kunlun in the Northern Tibetan Plateau. PhD Thesis Institute of Tibetan Plateau Research, Chinese Academy of Science p. 141 (in Chinese with English abstract).
Zhang, C.L., Ye, H.M., Wang, A.G., Guo, K.Y., Dong, Y.G., 2004. Geochemistry of the Neoproterozoic diabase and basalt in South of Tarim plate: evidence for the Neoproterozoic breakup of the Rodinia supercontinent in south of Tarim. Acta Petrologica Sinica 20, 473–482 (in Chinese with English abstract).
Zhang, Z.C., Xiao, X.C., Wang, J., Wang, Y., Kusky, T.M., 2008. Post-collisional Plio-Pleistocene shoshonitic volcanism in the western Kunlun Mountains, NW China: geochemical constraints on mantle source characteristics and petrogenesis. Journal of Asian Earth Sciences 31, 379–403.
Zhang, C.L., Li, Z.X., Li, X.H., Ye, H.M., 2009. Neoproterozoic mafic dyke swarms at the northern margin of the Tarim Block, NW China: age, geochemistry, petrogenesis and tectonic implications. Journal of Asian Earth Sciences 35, 167–179.
Zhao, Z., Mo, X., Dilek, Y., Niu, Y., DePaolo, D.J., Robinson, P., Zhu, D., Sun, C., Dong, G., Zhou, S., Luo, Z., Hou, Z., 2009. Geochemical and Sr–Nd–Pb–O isotopic compositions of the post-collisional ultrapotassic magmatism in SW Tibet: petrogenesis and implications for India intra-continental subduction beneath southern Tibet. Lithos 113, 190–212.
Zhao, J.M., Yuan, X.H., Liu, H.B., Kumar, P., Pei, S.P., Kind, R., Zhang, Z.J., Teng, J.W., Ding, L., Gao, X., Xu, Q., Wang, W., 2010. The boundary between the Indian and Asian tectonic plates below Tibet. Proceedings of the National Academy of Sciences of the United States of America 107, 11229–11233.
Zhao, W.J., Kumar, P., Mechie, J., Kind, R., Meissner, R., Wu, Z.H., Shi, D.N., Su, H.P., Xue, G.Q., Karplus, M., Tilmann, F., 2011. Tibetan plate overriding the Asian plate in central and northern Tibet. Nature Geoscience 4, 870–873.